

[This is a post-referring version]

[Accepted in *Remote Sensing of Environment*]

[DOI: 10.1016/j.rse.2019.111250]

[Link to the published paper: <https://doi.org/10.1016/j.rse.2019.111250>]

Surface albedo as a proxy for land-cover clearing in seasonally dry forests: Evidence from the Brazilian Caatinga

John Cunha^{a,*}, Rodolfo L. B. Nóbrega^{b,c}, Iana Rufino^d, Stefan Erasmi^e, Carlos Galvao^d, Fernanda Valente^f

^aFederal University of Campina Grande, Centre for the Sustainable Development of the Semi - Arid, Sumé, Brazil

^bUniversity of Reading, School of Archaeology, Geography and Environmental Science, Reading, United Kingdom

^cImperial College London, Faculty of Natural Sciences, Department of Life Sciences, Silwood Park Campus, Ascot, United Kingdom

^dFederal University of Campina Grande, Centre for Natural Resources and Technology, Campina Grande, Brazil

^eUniversity of Gottingen, Institute of Geography, Cartography GIS & Remote Sensing Section, Goettingen, Germany

^fUniversity of Lisbon, School of Agriculture, Forest Research Centre (CEF), Tapada da Ajuda, 1349-017 Lisbon, Portugal.

*Corresponding author: john.brito@ufcg.edu.br

Abstract:

Ongoing increase in human and climate pressures, in addition to the lack of monitoring initiatives, makes the Caatinga one of the most vulnerable forests in the world. The Caatinga is located in the semi-arid region of Brazil, and its vegetation phenology is highly dependent on precipitation, which has a high spatial and temporal variability. Under these circumstances, satellite image-based methods are valued due to their ability to uncover human-induced changes from climate effects on land cover. In this study, a time series stack of 670 Landsat images over a period of 31 years (1985–2015) was used to investigate spatial and temporal patterns of land-cover clearing (LCC) due to vegetation removal in an area of the Caatinga. We compared the performance of surface albedo (SA), the Enhanced Vegetation Index (EVI) and the Normalized Difference Vegetation Index (NDVI) and evaluated their suitability for monitoring LCC in contrast to precipitation-related variations. We applied a residual trend analysis (TSS-RESTREND), with detection of significant structural changes (breakpoints) to monthly Landsat time series. Our results show that SA was able to identify LCC with a higher accuracy (89%) than EVI (44%) and NDVI (46%). The overall outcome of the study shows the benefits of using spectral indices of Landsat time series that incorporate the short-wave infrared region, such as the SA, compared to vegetation indices for the monitoring of land-cover clearing, in seasonally dry forests such as the Caatinga.

Keywords: vegetation index; time series; Landsat; land-cover change; semi-arid.

[This is a post-referring version]

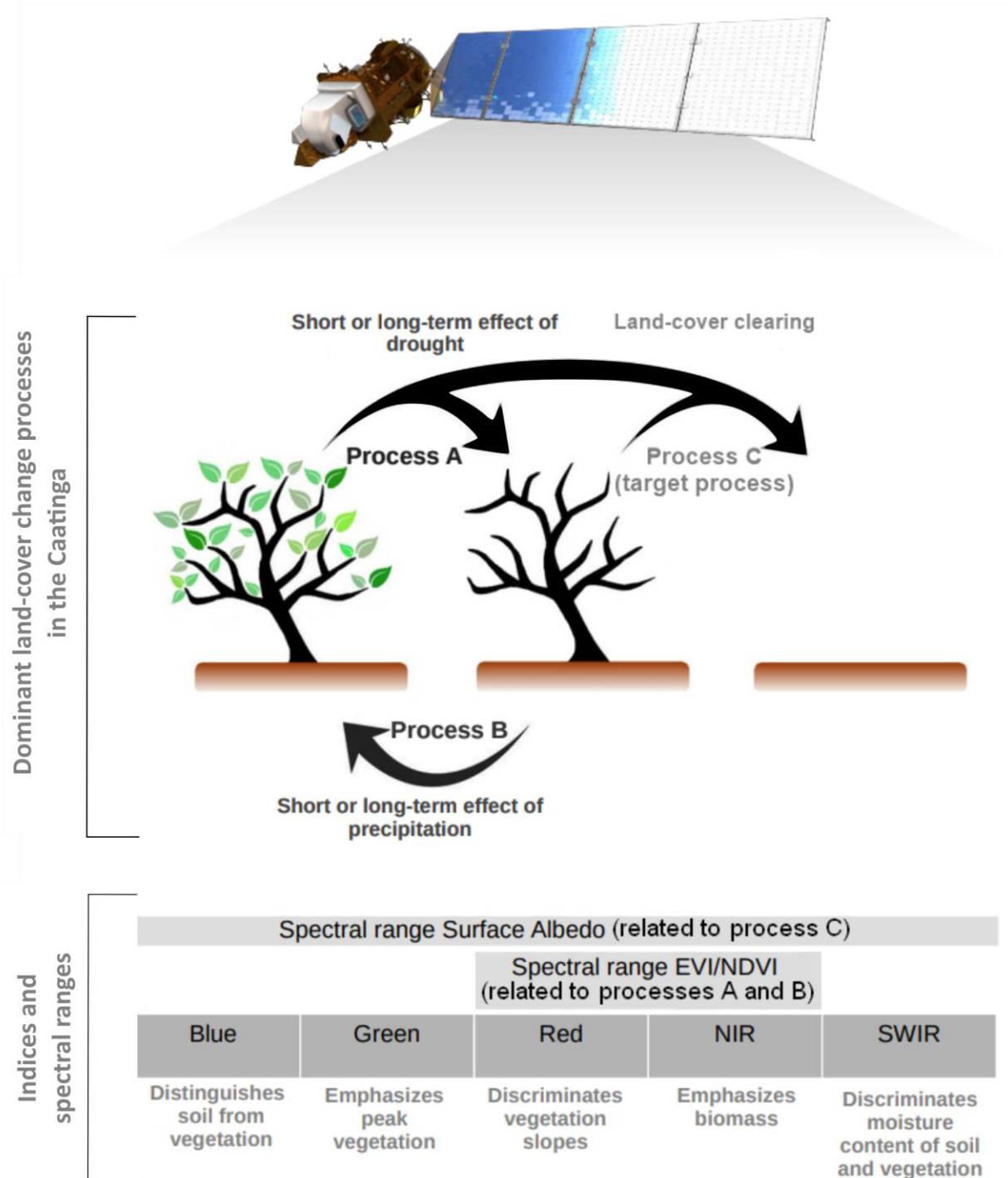
[Accepted in *Remote Sensing of Environment*]

[DOI: 10.1016/j.rse.2019.111250]

[Link to the published paper: <https://doi.org/10.1016/j.rse.2019.111250>]

43

Graphical abstract



44

[This is a post-referring version]

[Accepted in *Remote Sensing of Environment*]

[DOI: 10.1016/j.rse.2019.111250]

[Link to the published paper: <https://doi.org/10.1016/j.rse.2019.111250>]

45 1. Introduction

46 The identification of land-cover alteration driven by human action is one of the
47 main challenges when studying seasonally dry forests (Yang et al., 2016; Wessels et
48 al., 2007), as it is difficult to differentiate forest from non-forest areas (Mayes et al.,
49 2015). In these areas, vegetation greenness is strongly related to the annual
50 precipitation averages as well as the spatial variability and shifts of the rainy season
51 period within a year (Hein et al., 2011). This effect of temporal and spatial climatic
52 variability often masks the human actions in seasonally dry forests, especially after
53 long drought periods (Zhang et al., 2014), because the dry vegetation sustains an
54 extremely low level of photosynthetic material (Jacques et al., 2014), which is usually
55 used as an indicator of changes in land cover of forests (Eckert et al., 2015; Tucker
56 1979; Xu et al., 2014). However, even under these circumstances, forests lose a very
57 large proportion of the aboveground biomass when they are cleared (IPCC, 2000). The
58 identification of changes in terrestrial forest biomass on an annual basis is a
59 prerequisite for improving estimates of terrestrial water, energy, and carbon sources
60 and exchanges (Le Toan et al., 2011; Steyaert and Knox, 2008). Such assessment is
61 possible with time-series analysis, which is a widely accepted method to identify
62 vegetation clearing (Gómez et al., 2016; Song et al., 2014).

63 Long time series of satellite data are suitable to assess vegetation dynamics on
64 a regional scale (Schucknecht et al., 2013). In this context, Landsat data is one of the
65 most valuable sources of global observation. Owing to more than 30 years of medium-
66 resolution and multispectral data, Landsat datasets constitute the longest continuous
67 remotely-sensed record of the Earth's surface (Loveland and Dwyer, 2012). Despite

[This is a post-referring version]

[Accepted in *Remote Sensing of Environment*]

[DOI: 10.1016/j.rse.2019.111250]

[Link to the published paper: <https://doi.org/10.1016/j.rse.2019.111250>]

68 its low temporal resolution at 16 days, earlier problems in images' absolute geolocation
69 (Dwyer et al., 2018), and necessary adjustments of bidirectional reflectance effects
70 (Egorov et al., 2018), Landsat imagery quality has improved. Landsat dataset structure
71 provides information on radiometric, geometric and cloud cover quality to support
72 temporal analysis (Wulder et al., 2016). The higher-level products are freely available
73 through the United States Geological Survey (USGS) and allow users to retrieve
74 surface reflectance data (Ju and Masek, 2016).

75 Trend analysis of indices based on visible and near-infrared (VIS-NIR, 0.4-
76 1.1 μ m) wavelength ranges and computed from multi-year satellite data has been
77 widely and successfully used to monitor changes in vegetation productivity (Fensholt
78 et al. 2012; Higginbottom and Symeonakis, 2014; De Jong et al., 2012) and land
79 degradation (Li et al., 2016; Mariano et al., 2018). Although the effects of land-cover
80 clearing (LCC) on climate through changes in land surface biophysical processes are
81 well-documented, they also depend on the climate and vegetation background of the
82 region (Liu et al., 2016; Schwinning et al., 2004). The detection of LCC in seasonally
83 dry forests by using VIS-NIR, such as EVI and NDVI, is limited due to difficulties
84 distinguishing deciduous vegetation from the underlying ground during the dry period
85 (Daughtry, 2001; Jacques et al., 2014; Mayes et al., 2015; Nagler et al., 2000; Xu et
86 al., 2014). Zhao et al. (2018) highlight that while vegetation indices are routinely used
87 to monitor ecosystem attributes and functions such as vegetation cover and primary
88 productivity, the remote sensing-measured surface albedo (SA) can be used to assess
89 ecosystem status in drylands. SA is more sensitive to changes in biomass (Rodríguez-
90 Caballero et al., 2015); it has been used to monitor changes in dryland ecosystems,

[This is a post-referring version]

[Accepted in *Remote Sensing of Environment*]

[DOI: 10.1016/j.rse.2019.111250]

[Link to the published paper: <https://doi.org/10.1016/j.rse.2019.111250>]

91 and it is positively correlated with exposed soils (Yu et al., 2017), which are the
92 outcome of the LCC process (Lamchin et al., 2016; Liu et al., 2016;; Karnieli et al.,
93 2014). SA is also reported to be sensitive to seasonal phenological variations (Samain
94 et al., 2008; Wang et al., 2017), which are caused primarily by climatic variability in dry
95 forests.

96 Different statistical approaches based on satellite data have been used to
97 distinguish the effects of climatic variability on vegetation from anthropogenic actions
98 on land cover in seasonally dry forests (Anyamba et al., 2014; DeVries et al., 2015;
99 Evans and Geerken, 2004; Higginbottom and Symeonakis, 2014; Ibrahim et al., 2015;
100 Karlson and Ostwald, 2016; Leroux et al., 2017; Verbesselt et al., 2016). In most of
101 these studies, changes in the environment are identified by using trend analysis
102 methods that remove the seasonal cycle within the time series. Here, we highlight two
103 of them, considering their effectiveness to detect LCC in seasonally dry forests: the
104 RESidual TREND (RESTREND, Evans and Geerken, 2004; Li et al., 2016; Wessels et
105 al., 2012) and the Break detection For Additive Season and Trend (BFAST, DeVries
106 et al., 2015; Dutrieux et al., 2015; Verbesselt et al., 2012) methods. The RESTREND
107 method is capable of coping with inter-annual rainfall variability and trends for detection
108 of realistic levels of human-induced LCC by considering the residuals of the regression
109 between the target variable (e.g., NDVI) and rainfall (Wessels et al., 2012). The BFAST
110 method decomposes the time series for detecting structural changes in both the trend
111 and seasonal components to identify changes in land cover (De Jong et al., 2012). The
112 TSS-RESTREND (Time Series Segmentation and RESidual TREND) method (Burrell
113 et al., 2017) combines the RESTREND and BFAST analyses by attenuating seasonal

[This is a post-referring version]

[Accepted in *Remote Sensing of Environment*]

[DOI: 10.1016/j.rse.2019.111250]

[Link to the published paper: <https://doi.org/10.1016/j.rse.2019.111250>]

114 climate effects and detecting structural changes (breakpoints), and adds the Chow test
115 (Chow, 1960) to identify the most significant breakpoint in the time series. The Chow
116 test and the representation of the seasonal component by RESTREND are relevant
117 mechanisms incorporated into TSS-RESTREND to overcome the limitations of the
118 RESTREND and BFAST methods when each method is applied alone. As a result of
119 this combination and improvement, the TSS-RESTREND method can be divided into
120 two components: a structural change (breakpoint) detection and an overall trend
121 estimation. While the first one is feasible to detect changes that occur abruptly, such
122 as LCC, the latter is appropriate to identify trends that happen over a longer period of
123 time.

124 In our study, we focus on the use of the structural change detection component
125 of the TSS-RESTREND method in the Caatinga, which is a seasonally dry forest
126 constrained by climatic and anthropogenic pressures. Located in northeastern Brazil,
127 a region dominated by a semi-arid climate with high temporal and spatial rainfall
128 variability (Marengo et al., 2017), the Caatinga vegetation is a heterogeneous (Rodal
129 et al., 2008), seasonal semi-deciduous dry forest (Albuquerque et al., 2012; Brito et
130 al., 2012), with its phenology driven by short-term rainfall patterns (Erasmí et al., 2014;
131 Lima and Rodal, 2010). In this region, the human actions on the land cover have been
132 related to the clearing of the vegetation, and typically occurred at small spatial scales,
133 which can be better identified by using a higher spatial resolution (Lambin et al., 2003;
134 Stroppiana et al., 2012). However, most vegetation studies that analyse long (> 30
135 years) remote sensing time series use vegetation indices at low spatial resolution, i.e.,
136 1 to 8 km (Leroux et al., 2017), which is not sufficient to detect anthropogenic impacts

[This is a post-referring version]

[Accepted in *Remote Sensing of Environment*]

[DOI: 10.1016/j.rse.2019.111250]

[Link to the published paper: <https://doi.org/10.1016/j.rse.2019.111250>]

137 on land cover at higher resolutions (Munyati and Mboweni, 2013), such as the ones in
138 the Caatinga.

139 Our hypothesis was that the SA is a better indicator for LCC detection in
140 seasonally dry forests, such as the Caatinga, than other vegetation indices, here
141 represented by EVI and NDVI. Although the SA is known to show different responses
142 between vegetated and bare soil surfaces, its use to identify LCC in dry forests has
143 been poorly documented. We ascribe this scientific gap to the lack of global time-series
144 datasets that provide multispectral data and to only recent developments on trend
145 detection methods that translate the concept of abrupt LCC. In this study, this is
146 addressed by using a 31-year spectral Landsat monthly time series applied to the
147 structural change component of the TSS-RESTREND method in a Caatinga area that
148 has been under a multidecadal fragmented LCC process.

149 2. Study area and data

150 2.1. Study area

151 The study area is located in the Brazilian Caatinga, a seasonally tropical dry
152 forest that lies in northeastern Brazil (Fig. 1A). Unlike most seasonally dry tropical
153 forests that occur in isolated spots, the Caatinga spreads over a vast contiguous area,
154 occupying ca. 910,000 km² as the largest continuous seasonally dry tropical forest and
155 woodland vegetation (SDTFW) in the Americas (CNUC, 2017; Linares-Palomino et al.,
156 2011). Although it is a unique ecosystem with a high degree of biodiversity and number
157 of endemic species (Sobrinho et al., 2016), only 7.7% of its area is under environmental
158 protection by the Brazilian National System of Conservation Units, which is 1.3% of

[This is a post-referring version]

[Accepted in *Remote Sensing of Environment*]

[DOI: 10.1016/j.rse.2019.111250]

[Link to the published paper: <https://doi.org/10.1016/j.rse.2019.111250>]

159 restricted protection areas plus 6.4% of sustainable use areas (CNUC, 2017). The
160 Caatinga is considered the most neglected and threatened Brazilian major ecosystem
161 due to inadequate and unsustainable use of its natural resources over the past
162 decades (Moro et al., 2016). Native vegetated areas of the Caatinga have been cleared
163 mainly because of ill-planned land use, which is directly influenced by how the land is
164 used for living (Andrade-Silva et al., 2012; Araújo et al., 2007, 2010; Santos and
165 Tabarelli, 2002). In our study area, like many other parts of the Caatinga, this has been
166 commonly characterized by LCC caused by wood removal for firewood/charcoal
167 production (Leal et al., 2005; Sobrinho et al., 2016). Reforestation initiatives are rare
168 in the Caatinga and recuperation of the its vegetation in cleared areas is a challenge
169 because it may take several decades to naturally re-establish the original land cover
170 (Araujo et al., 2007; Lima et al., 2016; Pereira et al., 2003).

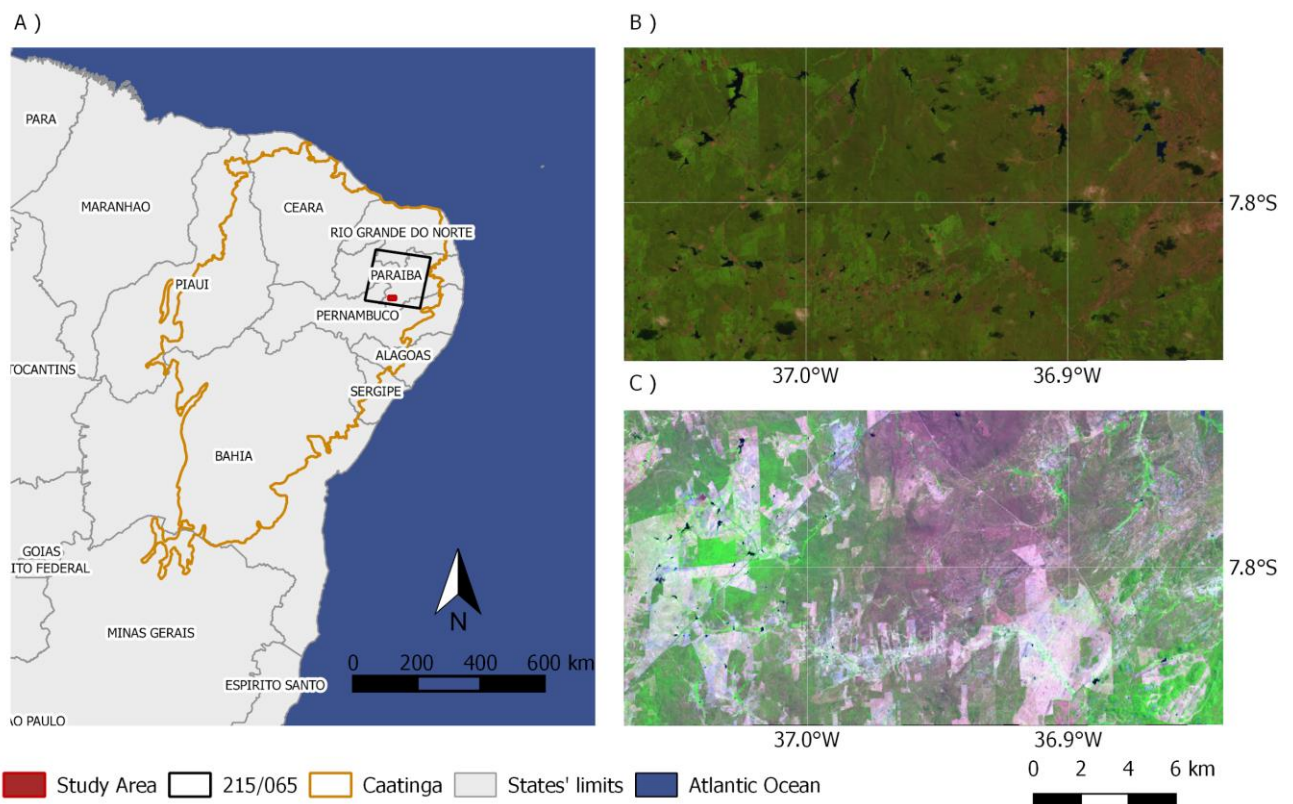


Fig. 1 - (A) Location of the Caatinga forest, Landsat scene 215/065 (path/row) and study area (Xmin: 37.07°W; Xmax: 36.84°W; Ymin: 7.86°S; Ymax: 7.74°S, WGS 84); (B) Landsat 5 false color composite (RGB to bands 4, 3 and 2) of the study area on 17/06/1984; (C) Landsat 8 false color composite (RGB to bands 5, 4 and 3) of the same area of (B) on 06/05/2015, showing land-cover differences between the first and last years of the studied period.

Our area of study is part of the *Depressão Sertaneja Meridional* ecoregion of the Caatinga, which is the largest of Caatinga's eight ecoregions, occupying ca. 45% of the entire Caatinga and considered to have the most typical Caatinga phytogeographic distribution (Andrade-Lima, 1981; Velloso et al., 2001; Moro et al., 2016). The region where our study area is located, known as *Cariris Velhos*, was selected and used for decades for studies on hydrology and soil conservation due to its representativeness of the climate, soil, geology, vegetation and topography for the Brazilian semiarid/Caatinga region (Cadier, 1996; Nouvelot, 1974; Padilha et al.,

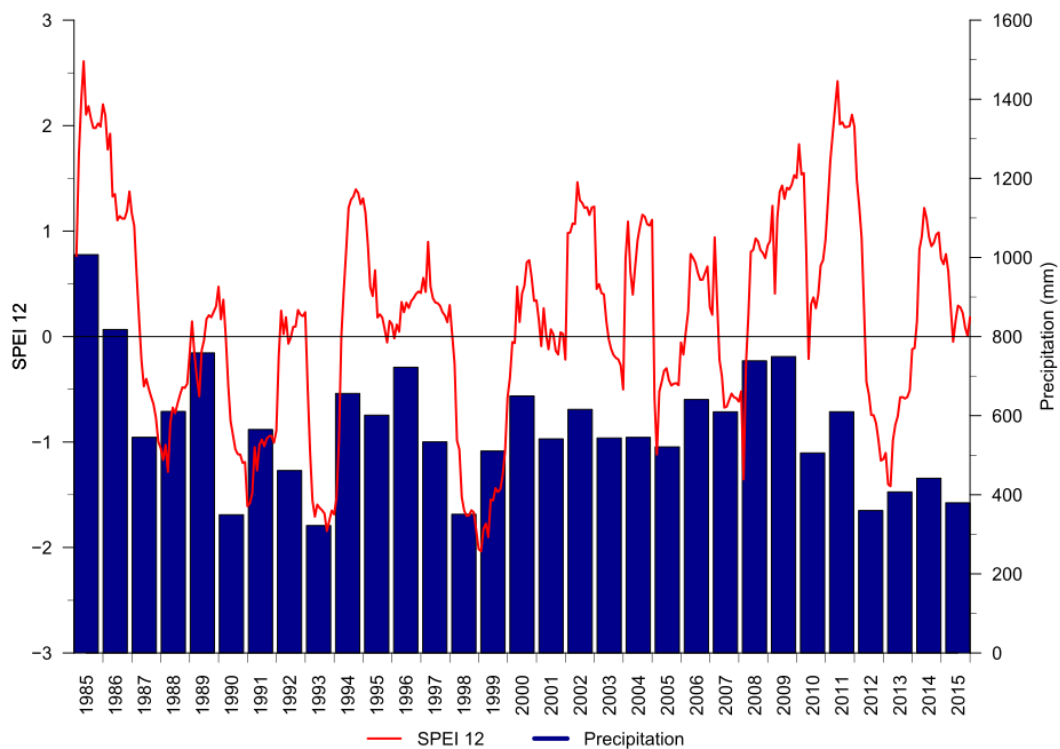
[This is a post-referring version]

[Accepted in *Remote Sensing of Environment*]

[DOI: 10.1016/j.rse.2019.111250]

[Link to the published paper: <https://doi.org/10.1016/j.rse.2019.111250>]

185 2016). This region is also included in one of the Caatinga's desertification nuclei, which
186 emphasize the application and need of our study in this type of area (Perez-Marin et
187 al., 2012). In this area, the main economic activities are livestock and subsistence
188 farming (Belchior et al., 2017), leading to substantial LCC (Fig. 1B and C). The climate
189 is hot semi-arid (BSh, Köppen classification) (Alvares et al., 2013), with only two
190 distinct seasons: the very hot rainy season (from February to May) and the hot dry
191 season (from June to January). The average annual rainfall in this region is
192 approximately 550 mm, with high interannual variability (coefficient of variation of
193 approximately 30%) and an average annual temperature of 23°C (Station code: 82792,
194 INMET, 2018). The Standard Precipitation-Evapotranspiration Index (SPEI, Vicente-
195 Serrano et al., 2010) for 12-month periods and the annual precipitation for the studied
196 period and area are shown in Fig. 2. SPEI is a drought index based on the difference
197 between precipitation and evapotranspiration that is usually used to detect and monitor
198 drought periods. For the study area, the SPEI shows that the alternation between dry
199 and wet periods have different magnitudes over the studied years.



200

201 Fig. 2 - The 12-month Standardized Precipitation-Evapotranspiration Index - SPEI 12 (source: Beguería
202 et al., 2017) and CHIRPS Precipitation (source: Funk et al., 2015) at geographic coordinates 36.75° W,
203 7.75° S (WGS 84).

204 2.2. Datasets

205 2.2.1. Landsat Surface Reflectance and Spectral Indices

206 In this study, we used the atmospherically corrected surface reflectance (SR)
207 from the Landsat satellites that are freely available by the United States Geological
208 Survey (<https://espa.cr.usgs.gov/>). SR data are generated at 30-meter spatial
209 resolution every 16 days. USGS provides the standard processing of SR including the
210 Level 1 Standard Terrain Correction, resulting in ortho-rectified images of high
211 geometric accuracy. Two different algorithms generate the SR data depending on the

[This is a post-referring version]

[Accepted in *Remote Sensing of Environment*]

[DOI: 10.1016/j.rse.2019.111250]

[Link to the published paper: <https://doi.org/10.1016/j.rse.2019.111250>]

212 measuring sensor: for Landsat 5 TM and Landsat 7 ETM+ the SR data are obtained
213 by the LEDAPS software (Masek et al., 2006), and for Landsat 8 OLI data are
214 processed by the LaSRC algorithm (Vermote et al., 2016).

215 We identified 670 available Landsat images between 1985 and 2015 that cover
216 our study area (390 from the TM sensor, 233 from the ETM+ and 47 from the OLI). For
217 our analysis we used the Landsat Surface Reflectance Quality Assessment (pixel_qa
218 band) to consider only clear pixels (values 66 and 130 for Landsat 5 and 7, or 322 and
219 386 for Landsat 8, USGS, 2018a,b), which represented in average 307 clear pixels per
220 grid cell for the 31-year time series.

221 The identification of LCC was obtained by using time series of NDVI (Tucker,
222 1979), EVI (Huete et al., 1997, 2002) and surface albedo (SA) (Shuai et al., 2014; Wang
223 et al., 2016). For each Landsat image, NDVI, EVI and SA were calculated using Eqs.
224 (1) to (3).

$$225 \quad NDVI = \frac{\rho_{NIR} - \rho_{RED}}{\rho_{NIR} + \rho_{RED}} \quad (1)$$

$$226 \quad EVI = 2.5 \times \frac{\rho_{NIR} - \rho_{RED}}{\rho_{NIR} + 6 \times \rho_{RED} - 7.5 \times \rho_{BLUE} + 1} \quad (2)$$

$$227 \quad SA = b_{BLUE} \times \rho_{BLUE} + b_{GREEN} \times \rho_{GREEN} + b_{RED} \times \rho_{RED} + b_{NIR} \times \rho_{NIR} + b_{SWIR1} \times \rho_{SWIR1} + \\ 228 \quad b_{SWIR2} \times \rho_{SWIR2} + b_0 \quad (3)$$

229 where ρ and b are the surface bidirectional reflectance values and their corresponding
230 conversion coefficients for the six non-thermal Landsat bands, i.e., blue, green, red,
231 NIR and the two shortwave infrared (SWIR1 and SWIR2) bands. Table 1 shows the b
232 values of several spectral bands of the three satellites used in this study.

233

234

[This is a post-referring version]

[Accepted in *Remote Sensing of Environment*]

[DOI: 10.1016/j.rse.2019.111250]

[Link to the published paper: <https://doi.org/10.1016/j.rse.2019.111250>]

235

236

237

238 Table 1 - Band conversion coefficients used to calculate shortwave albedo for the different Landsat data.

Sensor	b_{BLUE}	b_{GREEN}	b_{RED}	b_{NIR}	b_{SWIR1}	b_{SWIR2}	b_0
Landsat-5 TM	0.3206	0	0.1572	0.3666	0.1162	0.0457	- 0.0063
Landsat-7 ETM+	0.3141	0	0.1607	0.3694	0.1160	0.0456	- 0.0057
Landsat-8 OLI	0.2453	0.0508	0.1804	0.3081	0.1332	0.0521	0.0011

239 The highest values of the vegetation indices are found in vegetated areas, while
240 the lowest values occur in areas of bare soil (Mariano et al., 2018; Rodríguez-Caballero
241 et al., 2015; Zhao et al. 2018). As SA has an inverse behaviour of vegetation indices,
242 we used its complement to one ($1 - SA$) in the simulations, thus ensuring a pattern of
243 responses to LCC that corresponds to that of the vegetation indices EVI and NDVI.

244 Flood (2013) showed that the medoid (a multi-dimensional analogue of the
245 median) is a reliable measure to produce representative temporal image composites.
246 In this study, we used the median to reduce the initial time series (SA, EVI and NDVI)
247 to monthly composite images. Missing values were gap-filled by linear interpolation.
248 Further, a linear Savitzky–Golay filter was applied (Cao et al., 2018; Chen et al., 2004;
249 Savitzky and Golay, 1964), with a five-month half-width smoothing window in order to
250 reduce the noise caused by atmospheric variability.

[This is a post-referring version]

[Accepted in *Remote Sensing of Environment*]

[DOI: 10.1016/j.rse.2019.111250]

[Link to the published paper: <https://doi.org/10.1016/j.rse.2019.111250>]

251 2.2.2. Precipitation

252 The precipitation data used in this work were obtained from the Climate Hazards
253 group InfraRed Precipitation with Stations (CHIRPS) dataset (Funk et al., 2015;
254 Katsanos et al., 2016). CHIRPS is a near-global, very high spatial resolution (0.05°
255 grid) precipitation product developed for monitoring environmental changes over land
256 (Funk et al., 2015), which exhibited correlations ranging from 0.87 to 0.93 with rain
257 gauge observations in the Caatinga (Paredes-Trejo et al., 2017). We used monthly
258 precipitation data from October 1983 to December 2015.

259 3. Methods

260 3.1. TSS-RESTREND

261 The TSS-RESTREND method proposed by Burrell et al. (2017), combines the
262 RESTREND technique (Evans and Geerken, 2004) and the BFAST methodology
263 (Verbesselt et al., 2012, 2010), allowing a better and more accurate detection of
264 structural changes in the ecosystems. Prior to the application of trend analysis, it is
265 frequently necessary to remove the influence of exogenous random factors (e.g.,
266 rainfall, temperature) that, in addition to time and space, has a considerable effect on
267 the response variable. The removal process, either by parametric (e.g., regression) or
268 nonparametric (e.g., LOWESS) methods, reduces the variability of the studied variable
269 and increases the power to detect changes in it (Helsel and Hirsch, 2002; Schertz et
270 al., 1991). In remote sensing, a similar procedure has been applied for land-cover
271 analysis. The RESTREND method analyses the temporal trends in the vegetation
272 precipitation relationship (VPR) residuals from a linear regression of the NDVI on the

[This is a post-referring version]

[Accepted in *Remote Sensing of Environment*]

[DOI: 10.1016/j.rse.2019.111250]

[Link to the published paper: <https://doi.org/10.1016/j.rse.2019.111250>]

273 accumulated precipitation along a time period (Evans and Geerken, 2004). In Burrell
274 et al. (2017), VPR is obtained for two sets of information: complete NDVI time series
275 (CTS-NDVI) and annual maximum NDVI. In both cases, the linear regression uses the
276 Optimal Precipitation Accumulated (OPA) calculated on a per-pixel basis by an
277 exhaustive search algorithm, which combines different accumulation periods and lag
278 times. In our study, the OPA uses the CHIRPS precipitation data for accumulation
279 periods of 1–12 months and lag times of 0–3 months, resulting in an increase of 15
280 months at the beginning of the precipitation series. The optimum VPR is established
281 by finding the highest correlation coefficients between OPA and CTS-NDVI and
282 between OPA and annual maximum NDVI.

283 TSS-RESTREND uses annual VPR to exclude pixels that do not meet the
284 criteria to use the RESTREND method, i.e., a VPR that is significant, positive and
285 consistent with time (Wessels et al., 2012), and a gradual and consistent or monotonic
286 residuals' trend (Jamali et al., 2015), and then applies BFAST to CTS-VPR residuals
287 using the remaining pixels. The application of the BFAST method (Verbesselt et al.,
288 2010) returns a list of potential breakpoints that are analysed in a following step by the
289 Chow test (Chow, 1960) to determine if there is a significant breakpoint. After
290 identifying significant breakpoints, TSS-RESTREND calculates the significance of
291 each identified change and identifies the most significant breakpoint, if it exists, as the
292 structural change. More details on the TSS-RESTREND method can be found in
293 Burrell et al. (2017; 2018).

294 In our study, we applied the structural change (breakpoint) detection component
295 of the TSS-RESTREND method using the TSS.RESTREND package (Burrell et al.,

[This is a post-referring version]

[Accepted in *Remote Sensing of Environment*]

[DOI: 10.1016/j.rse.2019.111250]

[Link to the published paper: <https://doi.org/10.1016/j.rse.2019.111250>]

296 2017; <https://cran.r-project.org/package=TSS.RESTREND>) for the R software
297 environment (R Core Team, 2017). Although this method was initially used with NDVI
298 data (Burrell et al., 2017), we additionally applied it to SA and EVI. The original
299 TSS.RESTREND package was adapted to receive raster files as input.

300 3.2. Verification Methodology

301 The performance of the TSS-RESTREND method was evaluated at both
302 temporal and spatial levels. For each of the selected spectral indices and pixel, the
303 year of the most significant breakpoint was registered and compared with the actual
304 LCC year in order to evaluate the performance of SA, EVI and NDVI. The actual (true)
305 year of LCC was determined by visual analysis of RapidEye images from 2015, which
306 are freely available for academic use through the Brazilian Ministry of the Environment
307 (<http://geocatalogo.mma.gov.br/>), Landsat images (false color composite) and satellite
308 data from Google Earth Pro (<https://earth.google.com/>).

309 The validation dataset used in this work was built using a two-step procedure.
310 First, a detailed visual survey of recent (2015) RapidEye images allowed the
311 identification of several target areas where the original land cover had changed by the
312 complete removal of the vegetation (land-cover clearing). Then, Landsat images and
313 Google Earth Pro imagery were examined to determine the exact year of the LCC.
314 Both products provided at least one cloud-free composite image per year for the study
315 period and area at the altitude of visualization of 20 km. Additionally, several places
316 that had no visible human impact and that kept their original vegetation cover were
317 chosen as validation pixels. In October 2017, field visits to the study area were
318 conducted to confirm the land-cover status. Three different types of areas were

[This is a post-referring version]

[Accepted in *Remote Sensing of Environment*]

[DOI: 10.1016/j.rse.2019.111250]

[Link to the published paper: <https://doi.org/10.1016/j.rse.2019.111250>]

319 included in the validation dataset (Fig. 3): 1) 45 target areas of 120 m buffer each (ca.
320 80 pixels), 31 exhibit LCC in the period 1985–2015 and 14 show a preserved natural
321 vegetation; 2) a small region of 4.5 km² that has undergone a well-delimited time-space
322 land-cover clearing process over the 2003–2012 period, hereafter referred to as
323 "Subset I"; and 3) a region of 42 km² that has undergone a LCC process during 1985-
324 2015, hereafter referred to as "Subset II".

325 For each of the 45 selected target areas, the areal median of each spectral
326 index was calculated and the TSS-RESTREND was applied to the new generated time
327 series. From its outputs, only the results from the structural change detection
328 component were kept, namely the number of breakpoints and the estimate and
329 confidence interval of the date for each detected breakpoint (hereafter referred to as
330 estimated LCC year). Based on the statistical theory proposed by Bai (1997), the
331 breakpoints analysis implemented in the BFAST module (Verbesselt et al., 2010,
332 Zeileis et al., 2002) calculates confidence intervals for the change-point date with less
333 restrictive assumptions than those required by the usual parametric methods (i.e.,
334 independent and homogeneous normal errors). Due to these characteristics, these
335 intervals were used in the validation of our results. The output of the TSS-RESTREND
336 method was compared with the actual year of LCC. The accuracy of all indices was
337 computed as the ratio of the number of target areas that had their LCC (or the lack
338 thereof) correctly estimated to the total number of target areas. Other metrics related
339 to the lack of ability of detecting LCC when it actually took place and vice versa were
340 also evaluated. These metrics were divided into the following categories: a) *detected*
341 *true*, when the actual LCC year was contained in the 95% confidence interval of the

[This is a post-referring version]

[Accepted in *Remote Sensing of Environment*]

[DOI: 10.1016/j.rse.2019.111250]

[Link to the published paper: <https://doi.org/10.1016/j.rse.2019.111250>]

342 estimated LCC year, or when LCC was not detected and an actual LCC process did
343 not occur; b) *time wrong*, when the actual LCC year did not lie in the 95% confidence
344 interval of the estimated LCC year; c) *false negative*, when the LCC was not detected,
345 but it has actually occurred, and; d) *false positive*, when LCC was detected, but it has
346 not occurred.

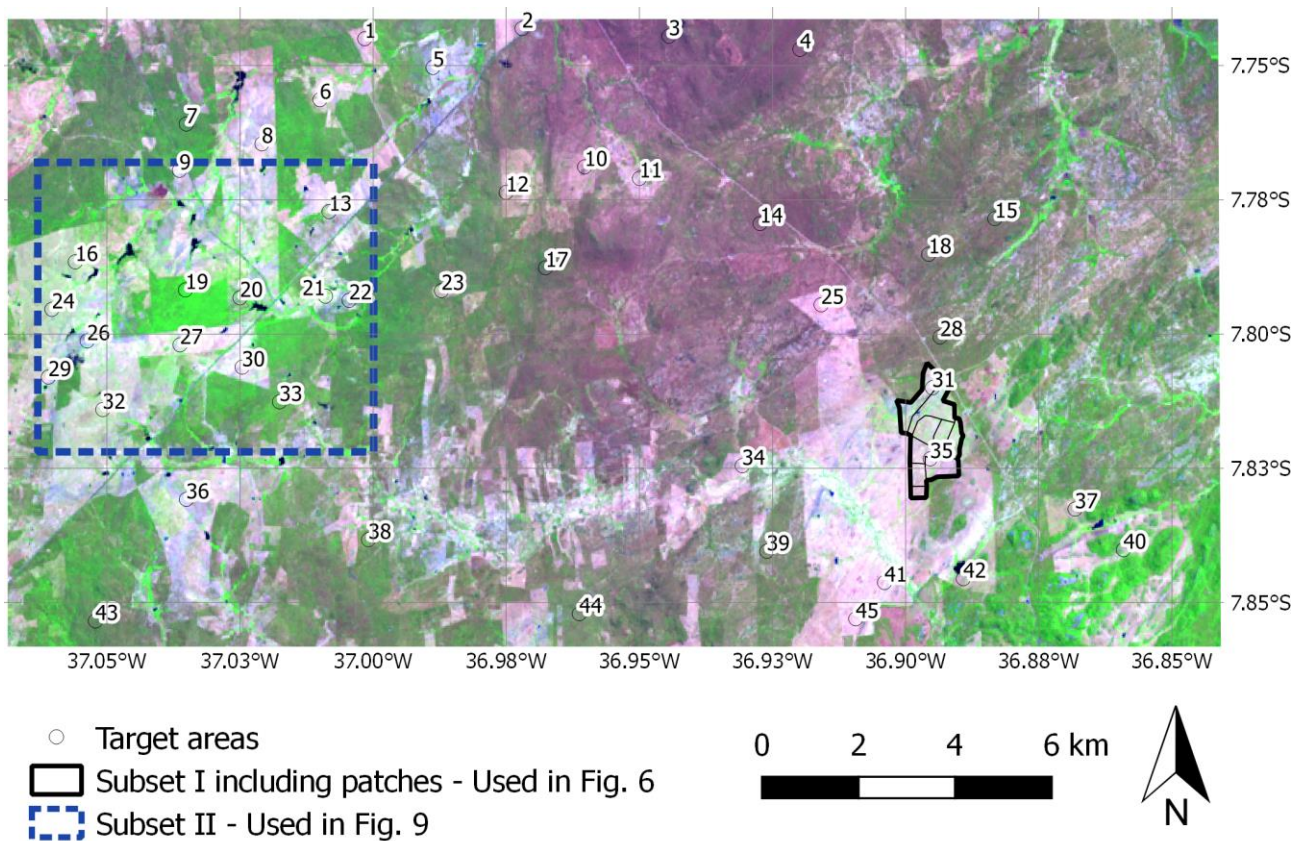
347 The Subset I illustrates the process of fragmentation of land-cover clearing and
348 the ability of the proposed methodology to identify these sequential changes (Fig. 3).
349 Within this area, pixels exhibiting land clearing in the same year were encompassed
350 within the same patch. In addition, the median was calculated for the estimated LCC
351 year of all pixels within each patch, providing a quantitative comparison with the actual
352 LCC year. The median rather than the mean was used as a summary measure
353 because it is a robust statistic of central tendency, less influenced by extreme values
354 (outliers). Additionally, the Kendall rank correlation coefficient (τ) between the median
355 of the estimated LCC year and the actual vegetation clearing year for the nine patches
356 was also calculated and its statistical significance tested. Subset II was used in a visual
357 analysis between the estimate breakpoint dates detected by SA time series and
358 Landsat images (false color composite) at 5-year intervals.

[This is a post-referring version]

[Accepted in *Remote Sensing of Environment*]

[DOI: 10.1016/j.rse.2019.111250]

[Link to the published paper: <https://doi.org/10.1016/j.rse.2019.111250>]



359

360 Fig. 3 - Location of the validation sites in the study area: 45 target areas (numbered, 31 target areas
361 where a LCC actually occurred and 14 areas with preserved natural vegetation), the Subset I that had
362 a sequential land-cover clearing process during 2003–2012 and the Subset II validation area. Source:
363 Landsat 8 false color composite (RGB to bands 5, 4 and 3).

364 4. Results

365 Our analyses show that the two main differences between SA, and EVI and
366 NDVI are the range of values (Fig 4), and the average number of breakpoints detected
367 by the structural change component of the TSS-RESTREND method (Table 2).
368 Whereas values ranged between 0.08 and 0.57 for EVI and 0.13 and 0.73 for NDVI,
369 SA values varied only between 0.10 and 0.25. Moreover, the number of the breakpoints
370 detected by using EVI and NDVI is greater than that with SA (Fig. 4). Most of the

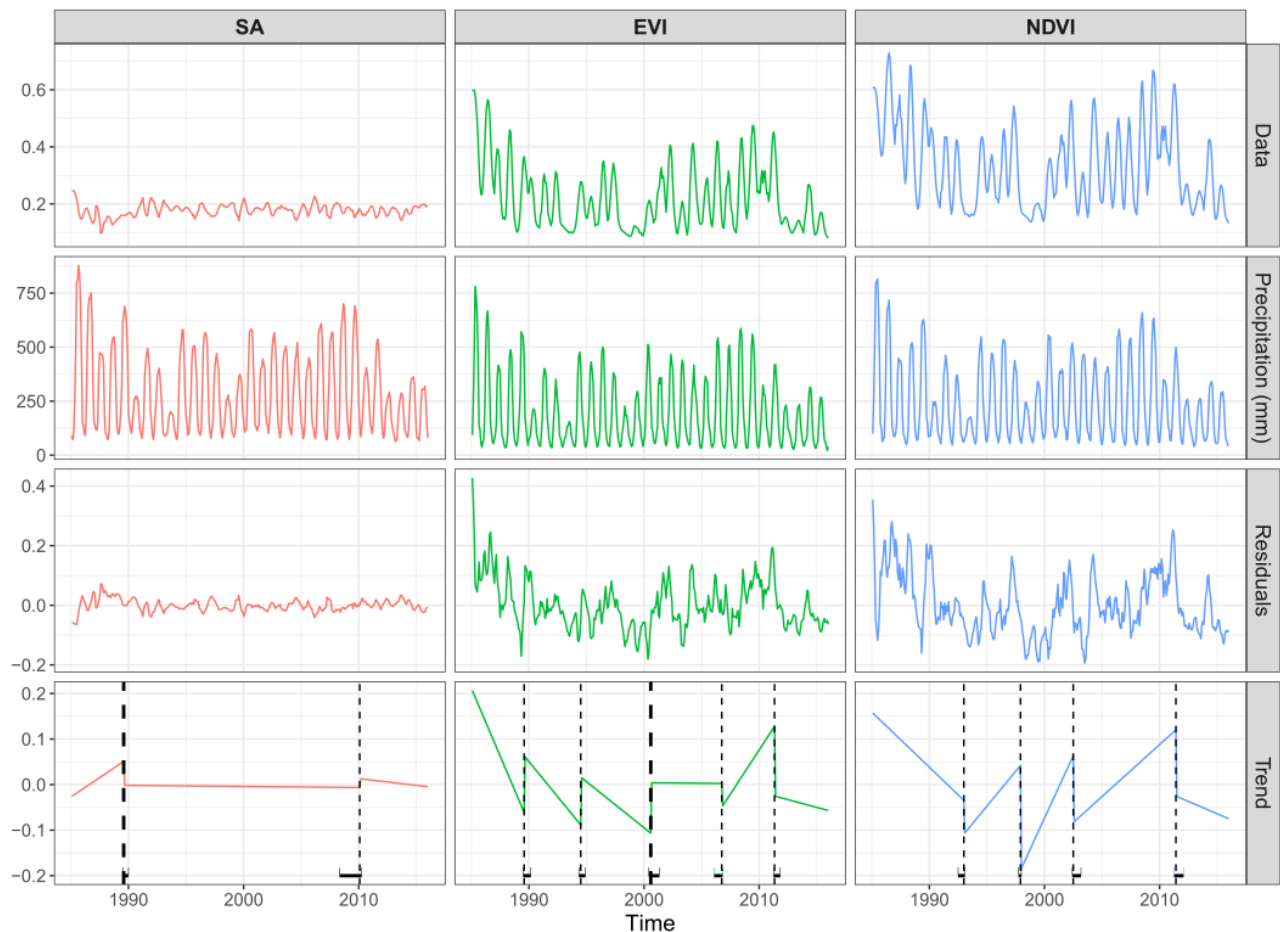
[This is a post-referring version]

[Accepted in *Remote Sensing of Environment*]

[DOI: 10.1016/j.rse.2019.111250]

[Link to the published paper: <https://doi.org/10.1016/j.rse.2019.111250>]

371 breakpoints occurred during a drought period (SPEI < -1, cf. Fig. 2), especially for EVI
372 and NDVI.

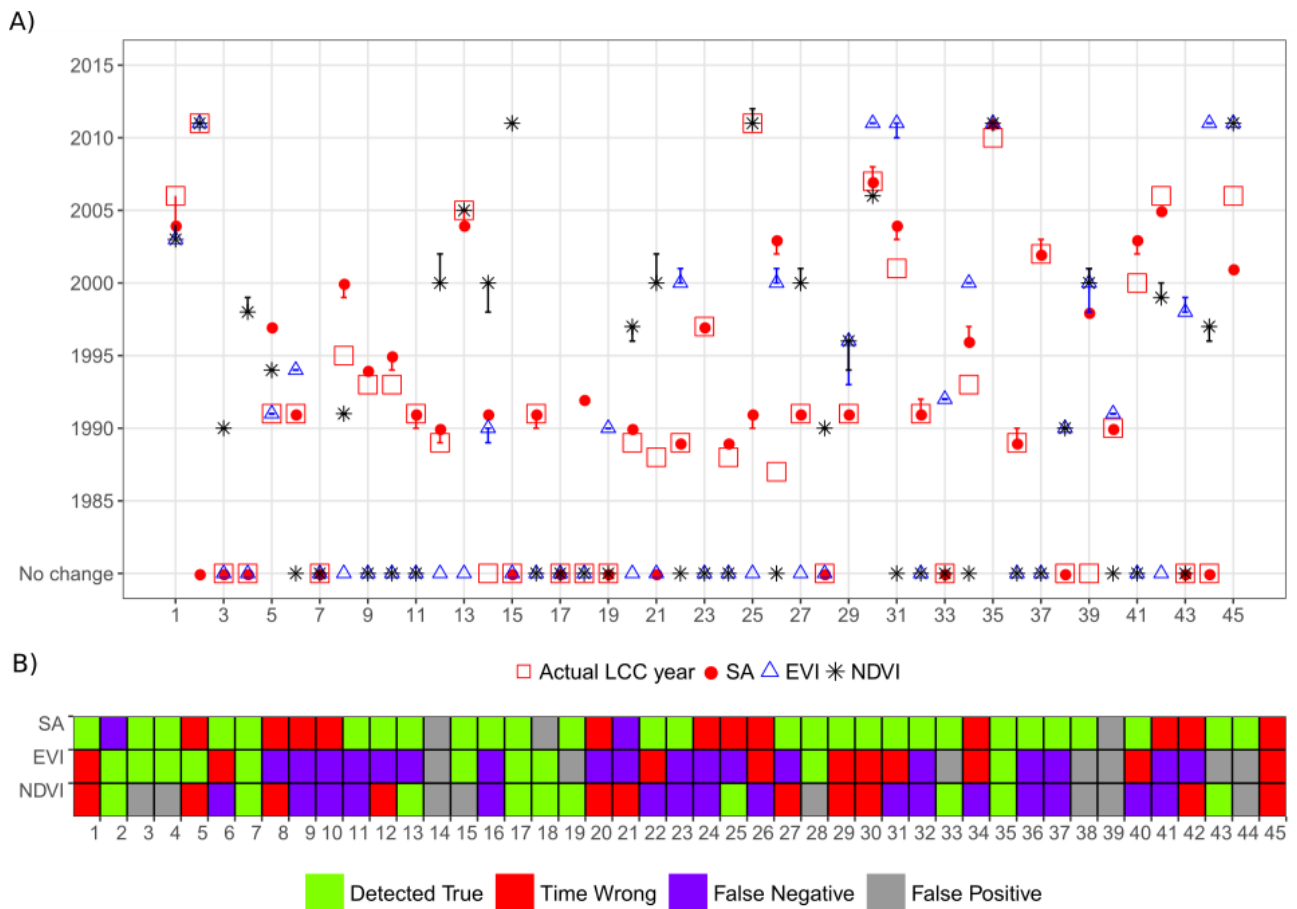


373

374 Fig. 4: TSS-RESTREND structural change detection outputs for the target area 22. Top row panel
375 shows SA, EVI and NDVI entire time series data, whereas the next panel has complete OPA time series,
376 followed by monthly residuals of OPA, and Trend to each time series spectral indices. In the Trend
377 panel, vertical lines represent breakpoints and the bold vertical line the most significant breakpoint.

378 In general, despite the smallest number of breakpoints identified by SA, this
379 index showed the best performance in detecting LCC on an annual scale and had on
380 average the narrowest 95% confidence interval for the breakpoint date when compared
381 to that of EVI and NDVI (Fig. 5, Table 2). The SA detected 89% of the LCC (being the
382 sum of detected true and time wrong), while EVI and NDVI detected only 44% and

383 46%, respectively (Table 2). The low performance of EVI and NDVI is reflected by the
384 great number of false negatives, representing 36–40%, whereas the false negatives
385 were only 4% for SA. The total false positives represented over 15% for EVI and NDVI,
386 and 7% for SA.



387

388 Fig. 5 – Estimated and actual year of land-cover clearing for SA, EVI and NDVI for the 45 target areas:
389 A) Description and B) Summary

390 The subset I is a region with LCC between 2001 and 2012 (highlighted in Fig. 3
391 within the black polygon) and it was used to analyse the results in more detail (Fig. 6).
392 This region contains two target areas, which exhibit contrasting performances: the LCC
393 in the target area 31 was only detected by the SA, while the LCC for target area 35
394 was correctly detected by all three indices (Fig 5). Within the polygon, the main

[This is a post-referring version]

[Accepted in *Remote Sensing of Environment*]

[DOI: 10.1016/j.rse.2019.111250]

[Link to the published paper: <https://doi.org/10.1016/j.rse.2019.111250>]

395 changes in land cover occurred between 2003 and 2012, which is shown by nine
396 patches. Each patch is identified by the actual LCC year that is dominant among its
397 pixels. The analysis of these patches revealed that when EVI and NDVI were used, a
398 substantial number of pixels (sometimes > 40%) were categorized as false negative
399 (Fig. 7A). This situation was particularly relevant in the patches where the LCC
400 occurred in 2003, 2004, 2008 and 2010 (Fig. 6 and 7A). In contrast, results obtained
401 with SA showed that false negative pixels were less than 10% for all patches (Fig. 7A)
402 and exhibited an overall better accuracy in identifying the actual LCC year (Fig. 7B). In
403 fact, for the nine patches, the median of the estimated LCC year by SA was closer to
404 the actual LCC year than those obtained with EVI and NDVI (Fig. 7B). This was also
405 confirmed by Kendall's correlation coefficient (τ) between actual and estimated LCC
406 years: SA had the highest value ($\tau = 0.86$) with the highest significance ($p < 0.01$).

407 Table 2 – Number of validation target areas in the different categories (and percentage of the total)
408 according to the results of the TSS-RESTREND method applied with the three spectral indices (Fig. 5),
409 average confidence interval amplitude and average number breakpoint detected.

Index	Detected True	Time Wrong	False Positive	False Negative	Average 95% Confidence Interval amplitude (in months)	Average number of Breakpoints Detected
SA	28 (62%)	12 (27%)	3 (7%)	2 (4%)	8.7	2.8
EVI	10 (22%)	10 (22%)	7 (16%)	18 (40%)	10.9	3.5
NDVI	10 (22%)	11 (24%)	8 (18%)	16 (36%)	11.6	4.0

410

411 The best performance of EVI and NDVI was observed for the patches where the
412 clearing of vegetation took place in 2011 and 2012 (Figs. 6 and 7). However, for the

[This is a post-referring version]

[Accepted in *Remote Sensing of Environment*]

[DOI: 10.1016/j.rse.2019.111250]

[Link to the published paper: <https://doi.org/10.1016/j.rse.2019.111250>]

413 other years and for a large number of pixels, the estimated LCC year was close to
414 years of a severe drought (1993 and 2000, cf. Fig. 2). The foremost detected
415 breakpoint years are the drought years of 1990 and 2000, and the period around 2010
416 (Fig. 7B and 8). Although there is a higher dispersion of the SA results than those of
417 EVI and NDVI, the median of the detected year of change is closer to the observed
418 date in the former index. Furthermore, while the validation polygon is hardly identified
419 in the output raster of these two vegetation indices, it is quite well-defined in the SA
420 raster (Fig. 6). This result is a consequence of the quite different performance of the
421 TSS-RESTREND method to detect LCC when applied to time series of the three
422 indices.

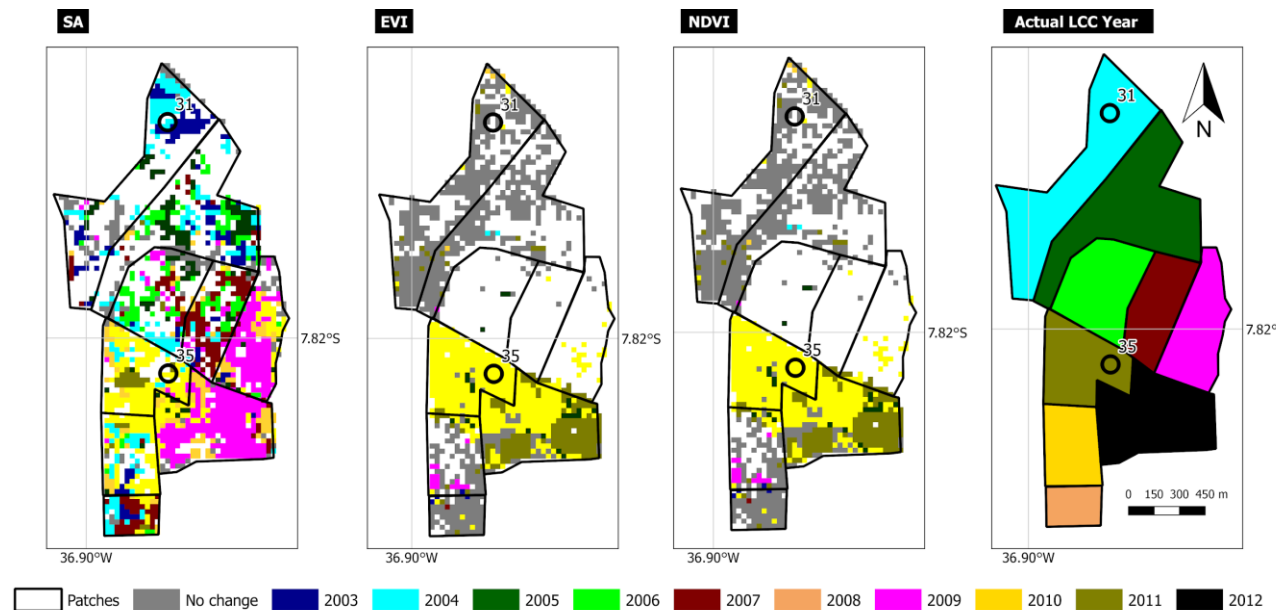
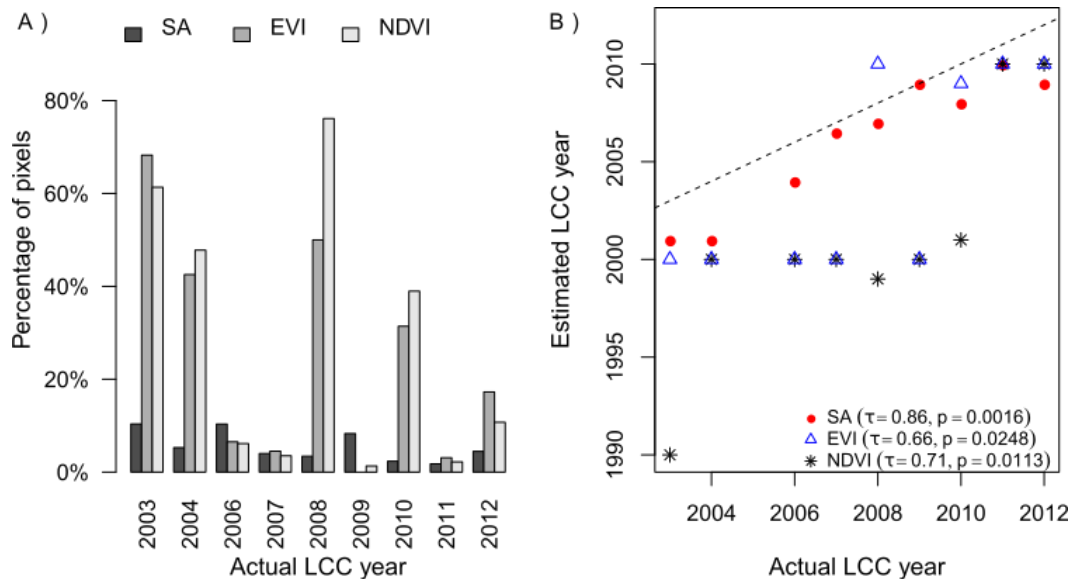


Fig. 6 – Polygon with selected patches showing the detected breakpoint years of LCC for SA, EVI, NDVI and actual LCC year.

Visual comparison of the breakpoint raster for the subset II with Landsat images false color composite shows that the SA has some difficulty in identifying the correct year of clearing when it occurs during the initial and final years of the time series (1985–

429 1990 and 2010–2015, Fig. 9). On the other hand, SA performed well for the small
430 vegetation areas that remain unchanged during the study period (e.g., the region were
431 the target area 19 is located), whereas with EVI and NDVI lower accuracy can be
432 interpreted as an effect of adverse climate period or degradation on the vegetation.
433 Although this ability of the NDVI and EVI might be useful to detect intra-annual changes
434 and trends of degradation of the vegetation, we have only assessed the skill of the
435 these indices to detect LCC.



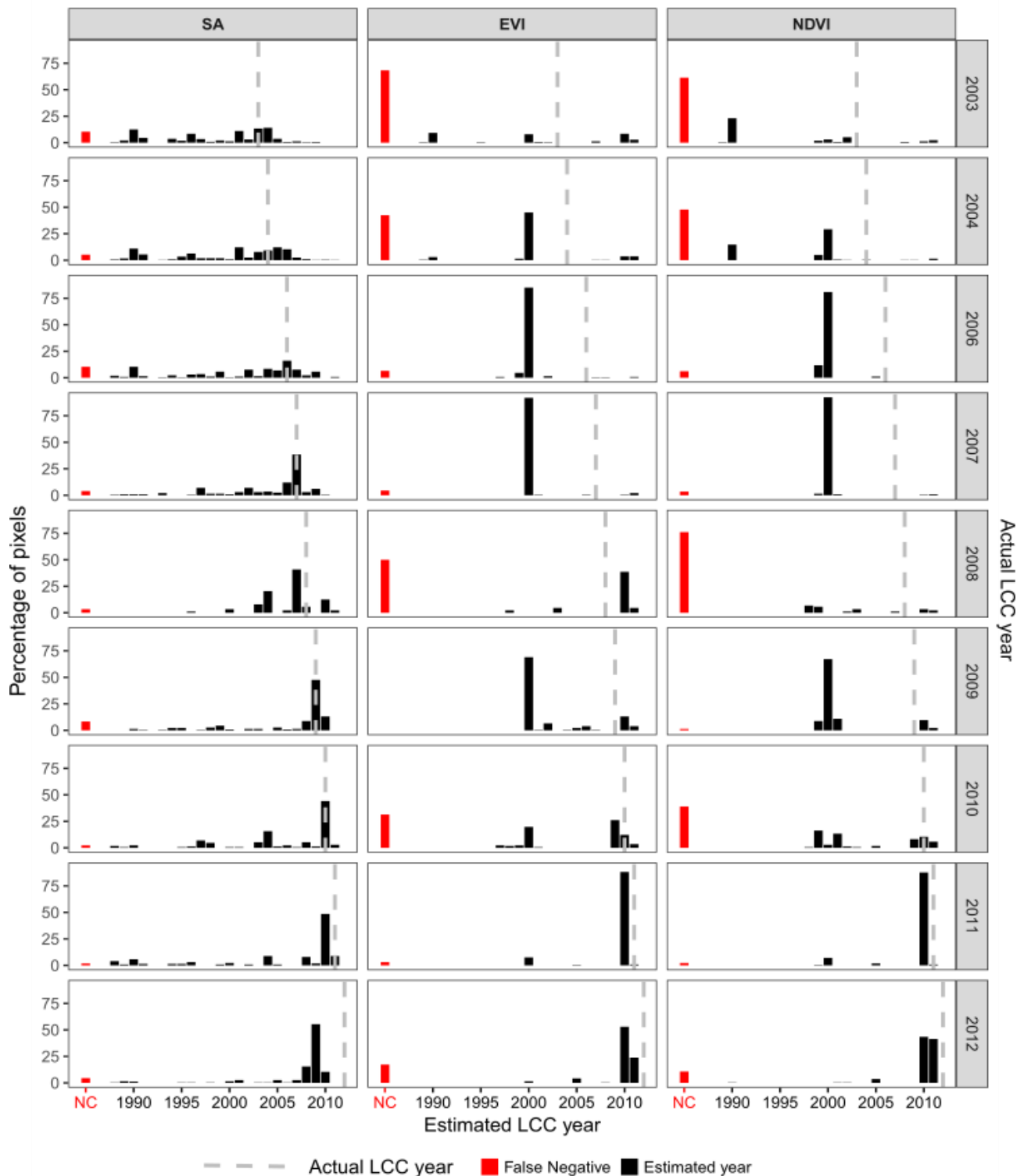
436
437 Fig. 7 - Observed change year of land-cover clearing of the different patches compared with the results
438 obtained with the TSS-RESTREND method for the SA, NDVI and EVI: A) percentage of the total number
439 of pixels in each patch where the method output was classified as False Negative; B) median of the
440 detected breakpoints within each of the nine patches for all the pixels where LCC was detected. The
441 dotted line is the 1:1 line and τ is the Kendall rank correlation coefficient.

[This is a post-referring version]

[Accepted in *Remote Sensing of Environment*]

[DOI: 10.1016/j.rse.2019.111250]

[Link to the published paper: <https://doi.org/10.1016/j.rse.2019.111250>]



442

443 Fig. 8 – Bar plots of the detected breakpoint year obtained by the TSS-RESTREND method applied to

444 the three spectral indices (SA, EVI and NDVI) for the different patches of the Subset I validation polygon.

445 Each patch is identified by the year of the actual vegetation clearing (also marked by the grey dashed

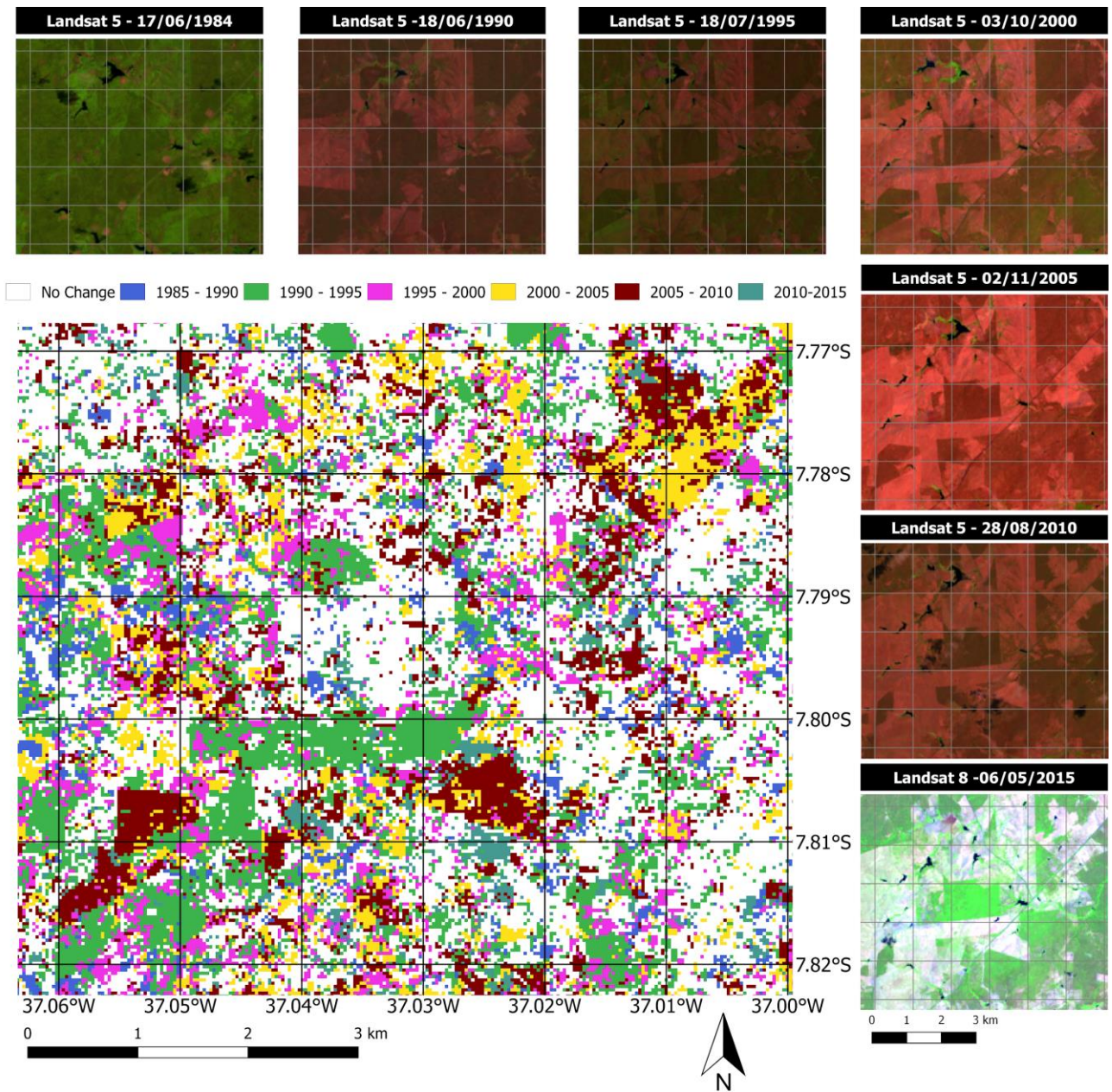
[This is a post-referring version]

[Accepted in *Remote Sensing of Environment*]

[DOI: 10.1016/j.rse.2019.111250]

[Link to the published paper: <https://doi.org/10.1016/j.rse.2019.111250>]

446 lines). The height of each black bar is the percentage of pixels where a change was detected in that
447 year. Red bars correspond to pixels where no change was detected.



448
449 Fig. 9 - Estimated LCC year by the TSS-RESTREND method applied to the SA time series for the Subset
450 II highlighted in Fig. 3. Images' source: Landsat 5 (RGB to 4, 3 and 2) and Landsat 8 (RGB to 5, 4 and
451 3) false color composite.

[This is a post-referring version]

[Accepted in *Remote Sensing of Environment*]

[DOI: 10.1016/j.rse.2019.111250]

[Link to the published paper: <https://doi.org/10.1016/j.rse.2019.111250>]

452 5. Discussion

453 Our study suggests that in the seasonally dry forests, especially the Brazilian
454 Caatinga, neither EVI nor NDVI are reliable spectral indices for identifying LCC due to
455 difficulties distinguishing deciduous vegetation from the underlying ground by indices
456 that use the VIS–NIR domain (Jacques et al., 2014; Mayes et al., 2015) during the dry
457 period. Despite the wide acceptance of using EVI (Dutrieux et al., 2015) and NDVI
458 (Leroux et al., 2017) to distinguish the effects of climate variability from anthropogenic
459 actions on changes in land cover, these indices exhibited a low performance in
460 detecting the correct timing of the LCC, as suggested by the TSS-RESTREND method.
461 Furthermore, for EVI and NDVI a high number of false negatives (cf. Table 2, Figs. 6
462 and 7A), and the matching between actual and estimated LCC years were less than
463 25%, which is far from an acceptable standard for detecting changes in land cover
464 (Aguirre-Gutiérrez et al., 2012; Mas, 1999).

465 The climate variability has a strong influence on EVI and NDVI in seasonally dry
466 forests (Guan et al 2015; Walker et al, 2015). Despite the TSS-RESTREND method
467 providing an approach to remove the effect of precipitation seasonality from the
468 indices, these vegetation indices still show an effect due to extended drought periods.
469 The years with the most severe droughts in the time series were 1990, 1993, 1998,
470 and 2012. When the LCC occurred in close proximity to these years, EVI and NDVI
471 exhibited a circumstantial good efficiency in identifying LCC, which was the case in
472 1990 and, especially, 2012. While 2011 was a wet year (maximum SPEI > 2.4), 2012
473 was the beginning of an extremely dry period, under drought conditions (SPEI < -0.5)
474 and with rainfall amounts below the total average (see Fig. 2).

[This is a post-referring version]

[Accepted in *Remote Sensing of Environment*]

[DOI: 10.1016/j.rse.2019.111250]

[Link to the published paper: <https://doi.org/10.1016/j.rse.2019.111250>]

475 SA exhibited a greater sensitivity to changes involving characteristics other than
476 the greenness of leaves because this index covers other bands (SWIR 1 and SWIR 2)
477 of the electromagnetic spectrum (Lui et al., 2017; Zhao et al., 2018), which are not
478 used by indices that use VIS-NIR. When a soil-plant-atmosphere system is altered by
479 an action of deforestation, the leafless woody biomass, which represents ca. 95% of
480 the aboveground biomass in the Caatinga (Silva and Sampaio, 2008), is removed and
481 consequently causes the total exposure of the soil to the effects of microclimate,
482 especially radiation, which can be detected by the SA. This response of the SA due to
483 LCC manifests regardless of the leaf status in the Caatinga. When the leafless
484 Caatinga vegetation is cleared, the Caatinga still loses its interseasonal shrub
485 structure, which causes abrupt and major decreases in surface roughness. As a
486 consequence of the LCC, the light attenuation, represented by the light extinction
487 coefficient and known to be substantial for deciduous shrublands (Aubin et al., 2000;
488 Domingo et al., 2000), is drastically decreased. By contrast, we could not identify any
489 pattern for the low performance in the detection of LCC for EVI and NDVI apart from
490 the climate. For these two indices, the estimated LCC year is often confined to a
491 moment near very dry periods. For example, 1990 was the first year with severe
492 drought conditions in our time series, and it was the estimated LCC year by either EVI
493 or NDVI for target points 3, 14, 19, 28 and 38, although no LCC actually occurred in
494 these areas.

495 Since soil moisture has a high influence on SA, the spectral signals from dry
496 and wet bare soil from any same site can be significantly different (He et al., 2014;
497 Matthias et al., 2000). Therefore, the variation of SA values should be interpreted with

[This is a post-referring version]

[Accepted in *Remote Sensing of Environment*]

[DOI: 10.1016/j.rse.2019.111250]

[Link to the published paper: <https://doi.org/10.1016/j.rse.2019.111250>]

498 caution when addressing LCC analysis. Like in most of the Caatinga region, the soils
499 of our study area are shallow and present a low water storage capacity (Medeiros et
500 al., 2018). When the land cover is cleared, the root zone storage is reduced, and, as a
501 result, SA increases. However, in soils with greater depth and water retention
502 capacities, SA may present lower performance as an indicator of LCC. Spectral indices
503 that use the NIR and the SWIR bands also show a better ability to detect plant
504 phenology than that of NDVI and EVI (Jin et al., 2013) by being more sensitive to the
505 water content of vegetation and soil (Rodríguez-Caballero et al., 2015, Zhao et al.,
506 2018). The spectral band SWIR provides a robust way to estimate the extent of bare
507 soil and vegetation cover in arid and semi-arid regions (Asner and Lobell, 2000).
508 Indices that use the SWIR domain, such as the Soil Tillate Index (STI) and Tasseled
509 Cap Wetness (TCW), showed good performance to identify the variance of dry masses
510 in the Sahel (Jacques et al., 2014) and LCC processes in southern Ethiopia (DeVries
511 et al., 2015). We ascribe to soil moisture the cause of the errors in detecting the actual
512 LCC year when using SA for the target areas 25 and 26. A substantial part of these
513 two areas are covered by ephemeral stream beds. Despite exhibiting no surface water
514 most of the years, the stream beds are known for acting as small aquifers by storing
515 water in the alluvial deposits and increasing the soil moisture along stream channels
516 (Fontes Junior and Montenegro, 2017).

517 The SA exhibited a high performance in detecting LCC (61%) or the lack of it
518 (79%), totalling an overall accuracy of 89% for all 45 target areas. For the target areas
519 where the LCC was detected, 39% of them were time wrong and only 6% were false
520 negatives. We attribute the imprecision in identifying the actual LCC year to some

[This is a post-referring version]

[Accepted in *Remote Sensing of Environment*]

[DOI: 10.1016/j.rse.2019.111250]

[Link to the published paper: <https://doi.org/10.1016/j.rse.2019.111250>]

521 adverse effects of the ecosystem response to LCC on the SA. After vegetation
522 removal, the remaining plant ecosystem, i.e., underground roots and soil, needs some
523 time to adapt to the new conditions (Saco et al., 2018), which can cause a gradual loss
524 of the root zone storage (D'Odorico et al., 2013), and, consequently, a delay in the full
525 bare soil SA response, which in turn will cause a time wrong for the estimated LCC
526 year that is after the actual one. Another aspect to consider is that some LCC activities
527 in the Caatinga occur at very small scales (e.g. activities on one-man farms) and they
528 might overlap two consecutive years until the disturbance in the target's SA exceed a
529 threshold that will qualify as a breakpoint in the time series analysis (Pineiro et al.,
530 2013). We believe that the target areas 9, 10, 20 and 24 exhibit a 1-year delay for the
531 detection of the actual LCC year. These four areas are located in the upper-left
532 quadrant in Fig. 3, and their LCC occurred between 1988 and 1993, which was a period
533 when this area was densely vegetated and its land cover was cleared after a highly
534 fragmented LCC process (see Fig. 9). If this 1-year delay is added to the confidence
535 interval of the estimated LCC years, the rate of the time wrong rate is reduced from 39
536 to 26%. This is a decrease of 40% in the time wrong estimates, whereas the same 1-
537 year delay tolerance only reduces 20% and 9% of EVI and NDVI time wrong LCC
538 estimates, respectively.

539 The TSS-RESTREND method was built upon two previous approaches to the
540 analysis of changes in land cover, i.e., BFAST and RESTREND, taking advantage of
541 their individual skills in one robust method. We used the structural change component
542 of the TSS-RESTREND, which has three main characteristics that were fundamental
543 to identify an efficient indicator of LCC in the Caatinga: the ability to (i) remove the

[This is a post-referring version]

[Accepted in *Remote Sensing of Environment*]

[DOI: 10.1016/j.rse.2019.111250]

[Link to the published paper: <https://doi.org/10.1016/j.rse.2019.111250>]

544 influence in the process of the main climatic variable, the precipitation, (ii) detect, within
545 the time series, structural significant changes in land cover, and (iii) select the most
546 significant of such changes. The TSS-RESTREND, a method conceived, developed
547 and validated to be used with vegetation indices, was evidenced as an efficient
548 approach to be used with SA. The combination of the TSS-RESTREND and SA was
549 appropriate to identify LCC in our Caatinga study area, where the clearing was followed
550 by subsistence farming or livestock occupation with only few underbrush or grass that
551 sustained the higher SA response, qualifying the clearing as the most significant
552 breakpoint in the time series analysis of the TSS-RESTREND. The slow
553 reestablishment of native vegetation on bare soil areas upon abandonment is due to
554 the low natural fertility condition of the shallow, heterogeneous soils of the Caatinga
555 (Salcedo et al., 1997; Sobrinho et al, 2016) and adverse climate (Althoff et al., 2016)

556 The two false negatives (in the target areas 2 and 21) detected by the SA
557 represented areas that had their vegetation removed in either the first or last five years
558 of the time series, i.e., 1985–1990 and 2010–2015. In these intervals, when using SA,
559 the TSS-RESTREND method shows limitations in establishing a breakpoint. As in
560 other time series analysis methods, errors at the beginning and at the end of any finite-
561 length time series is a common issue (Torrence and Compo, 1998). The statistical
562 theory that supports BFAST (Bai, 1997; Verbesselt et al., 2010), one of the main
563 components of the TSS-RESTREND, requires that a minimum amount of data is set
564 between successive breakpoints and at the beginning and the end of the times series
565 to be able to identify a structural change. Besides, the conclusion of a statistical
566 hypothesis test (e.g., the Chow test) based on a small sample can be unreliable

[This is a post-referring version]

[Accepted in *Remote Sensing of Environment*]

[DOI: 10.1016/j.rse.2019.111250]

[Link to the published paper: <https://doi.org/10.1016/j.rse.2019.111250>]

567 because the null hypothesis (corresponding to a non-significant breakpoint) will hardly
568 be rejected at the standard significance levels. Therefore, the use of long time series
569 is essential to reduce these types of uncertainties. In our study, most of the LCC
570 occurred in the 1990s after the first five years of the time series. The Landsat dataset
571 was a valuable source of information by providing long time series where these LCC
572 processes could be evaluated free from these edge effects.

573 Our study supports further research towards a better understanding of Caatinga
574 land-cover dynamics. When considering the scale at which these biophysical variations
575 can impact large ecosystem extensions such as the Caatinga, not only the carbon
576 balance is affected, but also the energy and water balances (Bonan, 2008). Although
577 the LCC causes a radiative cooling effect due to the increase of SA, this is unbalanced
578 by the associated decrease in evapotranspiration and in surface roughness
579 (Sanderson et al., 2012), which has consequences to regional and global climate, as
580 evidenced by model experiments (Perugini et al., 2017). Based on our work, further
581 analysis and developments in this direction should consider: (i) a deep analysis of SA
582 and other spectral bands applications in LCC studies in other seasonal tropical dry
583 forests; (ii) a cross-related analysis of SA and other variables, such as biomass,
584 evapotranspiration and soil moisture, supported by remote sensing data, and; (iii) the
585 suitability of TSS-RESTREND method in identifying other type of land-cover change
586 processes, such as degradation and fragmentation, not directly covered in our study.

587 6. Conclusions

588 We applied SA, EVI and NDVI to the TSS-RESTREND method by using a 31-
589 year Landsat time series to evaluate the performance of these indices to detect LCC

[This is a post-referring version]

[Accepted in *Remote Sensing of Environment*]

[DOI: 10.1016/j.rse.2019.111250]

[Link to the published paper: <https://doi.org/10.1016/j.rse.2019.111250>]

590 in the Brazilian Caatinga, a tropical seasonally dry forest. We found that SA exhibited
591 a higher accuracy than the EVI and NDVI, and that the structural change detection
592 component of the TSS-RESTREND method was appropriate to identify the LCC.

593 The spatial resolution and long-term series of the Landsat images allowed a
594 systematic assessment of altered targets on the land surface, laid out in a complex
595 and fragmented pattern characteristic of the anthropogenic LCC in our studied area.
596 TSS-RESTREND showed a satisfactory performance in using long-term satellite data
597 to identify LCC in the Caatinga. The concept of this method is compatible with the
598 reality of the land cover dynamics in this seasonally dry forest, since the selection of
599 the most significant breakpoint unveils the LCC without subsequent vegetation
600 reestablishment. We found some imprecision in the method to identify LCC with a false
601 negative in the first and last few years of the time series (i.e., 1985–1990 and 2010–
602 2015).

603 For the two different validation datasets used in this study (target areas and
604 subset I), the SA presented an overall better performance than NDVI and EVI, being
605 able to detect LCC with an acceptable accuracy. The lower performance of the EVI
606 and NDVI indices in the detection of LCC in the Caatinga is explained by their high
607 sensitivity to leaf cover variations as a result of seasonal or extreme dry conditions.
608 Changes in land cover affect the entire soil-plant-atmosphere system, such as removal
609 of biomass and changes in soil properties, as well as in the microclimate, due to direct
610 exposure to radiation, precipitation and wind. Based on those changes, studies should
611 not rely only on vegetation indices but also look for other spectral ranges that will better
612 represent the peculiar characteristics of specific ecosystems.

[This is a post-referring version]

[Accepted in *Remote Sensing of Environment*]

[DOI: 10.1016/j.rse.2019.111250]

[Link to the published paper: <https://doi.org/10.1016/j.rse.2019.111250>]

613 Acknowledgments

614

615 This work has been funded by the Brazilian National Council for Scientific and
616 Technological Development (grant numbers 490115/2013-6 and 310789/2016-8) and
617 the European Commission (grant number FP7-614048) through the EUBrazilCC
618 project (<http://eubrazilcloudconnect.eu/>), CAPES-ANA (grant number
619 88887.115880/2015-01), and CAPES/PDSE (grant number 88881.134740/2016-01).
620 This work also forms part of the UK/Brazil Nordeste project funded jointly through the
621 UK Natural Environment Research Council (NE/N012526/1 ICL and NE/N012488/1
622 UoR) and the Fundação de Amparo à Pesquisa do Estado de São Paulo (2015/50488-
623 5). We would like to thank the constructive feedback from the reviewers. The Forest
624 Research Centre (CEF) is a research unit funded by Fundação para a Ciência e a
625 Tecnologia I.P. (FCT), Portugal (UID/AGR/00239/2013).

626

627 References

- 628 Aguirre-Gutiérrez, J., Seijmonsbergen, A.C., Duivenvoorden, J.F., 2012. Optimizing land cover
629 classification accuracy for change detection, a combined pixel-based and object-based
630 approach in a mountainous area in Mexico. *Appl. Geogr.* 34, 29–37.
631 doi:10.1016/j.apgeog.2011.10.010
- 632 Albuquerque, U.P., de Lima Araújo, E., El-Deir, A.C.A., de Lima, A.L.A., Souto, A., Bezerra, B.M.,
633 Ferraz, E.M.N., Maria Xavier Freire, E., Sampaio, E.V. de S.B., Las-Casas, F.M.G., de
634 Moura, G.J.B., Pereira, G.A., de Melo, J.G., Alves Ramos, M., Rodal, M.J.N., Schiel, N., de
635 Lyra-Neves, R.M., Alves, R.R.N., de Azevedo-Júnior, S.M., Telino Júnior, W.R., Severi, W.,
636 2012. Caatinga Revisited: Ecology and Conservation of an Important Seasonal Dry Forest,
637 *The Scientific World Journal*. doi:10.1100/2012/205182
- 638 Alvares, C.A., Stape, J.L., Sentelhas, P.C., De Moraes Gonçalves, J.L., Sparovek, G., 2013.
639 Köppen's climate classification map for Brazil. *Meteorol. Zeitschrift* 22, 711–728.
640 doi:10.1127/0941-2948/2013/0507
- 641 Althoff, T. D., Menezes, R. S. C., de Carvalho, A. L., de Siqueira Pinto, A., Santiago, G. A. C.
642 F., Ometto, J. P. H. B., Sampaio, E. V. (2016). Climate change impacts on the
643 sustainability of the firewood harvest and vegetation and soil carbon stocks in a tropical

[This is a post-referring version]

[Accepted in *Remote Sensing of Environment*]

[DOI: 10.1016/j.rse.2019.111250]

[Link to the published paper: <https://doi.org/10.1016/j.rse.2019.111250>]

- 644 dry forest in Santa Teresinha Municipality, Northeast Brazil. *Forest Ecology and*
645 *Management*, 360, 367–375. doi:10.1016/j.foreco.2015.10.001
- 646 Andrade-Lima, D, 1981. The caatinga dominium. *Revista brasileira de Botânica*, 4, 149-163.
- 647 Andrade-Silva, A.C.R., Nemésio, A., de Oliveira, F.F., Nascimento, F.S., 2012. Spatial-Temporal
648 Variation in Orchid Bee Communities (Hymenoptera: Apidae) in Remnants of Arboreal
649 Caatinga in the Chapada Diamantina Region, State of Bahia, Brazil. *Neotrop. Entomol.*
650 41, 296–305. doi:10.1007/s13744-012-0053-9
- 651 Anyamba, A., Small, J.L., Tucker, C.J., Pak, E.W., 2014. Thirty-two Years of Sahelian Zone
652 Growing Season Non-Stationary NDVI3g Patterns. *Remote Sens.* 6, 3101–3122.
653 doi:10.3390/rs6043101
- 654 Araújo, E.L., Castro, C.C., Albuquerque, U.P., 2007. Dynamics of Brazilian Caatinga – A Review
655 Concerning the Plants, Environment and People. *Funct. Ecosyst. Communities* 1, 15–28.
- 656 Araújo, V.F.P., Bandeira, a G., Vasconcellos, a, 2010. Abundance and stratification of soil
657 macroarthropods in a Caatinga Forest in Northeast Brazil. *Braz. J. Biol.* 70, 737–46.
658 doi:10.1590/S1519-69842010000400006
- 659 Asner, G. P., & Lobell, D. B. (2000). A Biogeophysical Approach for Automated SWIR Unmixing
660 of Soils and Vegetation. *Remote Sensing of Environment*, 74(1), 99–112.
661 doi:10.1016/s0034-4257(00)00126-7
- 662 Aubin, I., Beaudet, M., Messier, C., 2000. Light extinction coefficients specific to the
663 understory vegetation of the southern boreal forest, Quebec *Can. J. For. Res.* 30: 168–
664 177
- 665 Bai, J., 1997. Estimation of a Change Point in Multiple Regression Models. *Rev. Econ. Stat.* 79,
666 551–563. doi:10.1162/003465397557132
- 667 Begueria, S., Latorre, B., Reig, F., Vicente-Serrano, S.M. 2017. Global SPEI database.
668 <http://spei.csic.es/database.html>. Access in 11 January 2017.
- 669 Belchior, M., Tai, D.W., Held, F.C. Von, 2017. Indicadores IBGE. *Inst. Bras. Geogr. E Estatística*
670 - Ibge 6.
- 671 Bonan, G. B., (2008) Forests and climate change: Forcings, feed- backs, and the climate
672 benefits of forests. *Science*, 320, 1444– 1449, doi:10.1126/science.1155121.
- 673 Brito, A.F., Presley, S.J., Santos, G.M.M., 2012. Temporal and trophic niche overlap in a guild
674 of flower-visiting ants in a seasonal semi-arid tropical environment, *Journal of Arid*
675 *Environments*. doi:10.1016/j.jaridenv.2012.07.001
- 676 Burrell, A.L., Evans, J.P., Liu, Y., 2017. Detecting dryland degradation using Time Series
677 Segmentation and Residual Trend analysis (TSS-RESTREND). *Remote Sens. Environ.*
678 doi:10.1016/j.rse.2017.05.018
- 679 Burrell, A.L., Evans, J.P., Liu, Y., 2018. The impact of dataset selection on land degradation
680 assessment. *ISPRS J. Photogramm. Remote Sens.* 146, 22-37. doi:
681 10.1016/j.isprsjprs.2018.08.017

[This is a post-referring version]

[Accepted in *Remote Sensing of Environment*]

[DOI: 10.1016/j.rse.2019.111250]

[Link to the published paper: <https://doi.org/10.1016/j.rse.2019.111250>]

- 682 Cadier, E. 1996. Small watershed hydrology in semi-arid north-eastern Brazil: basin typology
683 and transposition of annual runoff data. *Journal of Hydrology*, 182(1–4), 117–141. doi:
684 10.1016/0022-1694(95)02933-8
- 685 Cao, R., Chen, Y., Shen, M., Chen, J., Zhou, J., Wang, C., & Yang, W. 2018. A simple method to
686 improve the quality of NDVI time-series data by integrating spatiotemporal information
687 with the Savitzky-Golay filter. *Remote Sensing of Environment*, 217, 244–257.
688 doi:10.1016/j.rse.2018.08.022
- 689 Chen, J., Jönsson, P., Tamura, M., Gu, Z., Matsushita, B., Eklundh, L., 2004. A simple method
690 for reconstructing a high-quality NDVI time-series data set based on the Savitzky-Golay
691 filter. *Remote Sens. Environ.* 91, 332–344. doi:10.1016/j.rse.2004.03.014
- 692 Chow, G.C., 1960. Tests of equality between sets of coefficients in two linear regressions.
693 *Econometrica* 28:591–605. doi:10.2307/1910133.
- 694 CNUC - Cadastro Nacional de Unidades de Conservação (Brazilian National Database of
695 Conservation Units). Accessed in oct-2018
- 696 D’Odorico, P., Bhattachan, A., Davis, K.F., Ravi, S., Runyan, C.W., 2013. Global desertification:
697 Drivers and feedbacks. *Adv. Water Resour.* 51, 326–344.
698 doi:10.1016/j.advwatres.2012.01.013
- 699 Daughtry, C.S.T., 2001. Discriminating Crop Residues from Soil by Shortwave Infrared
700 Reflectance. *Agron. J.* 93, 125. doi:10.2134/agronj2001.931125x
- 701 De Jong, R., Verbesselt, J., Schaepman, M.E., de Bruin, S., 2012. Trend changes in global
702 greening and browning: Contribution of short-term trends to longer-term change. *Glob.*
703 *Chang. Biol.* doi:10.1111/j.1365-2486.2011.02578.x
- 704 DeVries, B., Verbesselt, J., Kooistra, L., Herold, M., 2015. Robust monitoring of small-scale
705 forest disturbances in a tropical montane forest using Landsat time series. *Remote Sens.*
706 *Environ.* doi:10.1016/j.rse.2015.02.012
- 707 Domingo, F., Villagarcia, L., Brenner, A. J., & Puigdefabregas, J. 2000. *Measuring and modelling*
708 *the radiation balance of a heterogeneous shrubland. Plant, Cell and Environment*, 23(1),
709 27–38. doi:10.1046/j.1365-3040.2000.00532.x
- 710 Dutrieux, L.P., Verbesselt, J., Kooistra, L., Herold, M., 2015. Monitoring forest cover loss using
711 multiple data streams, a case study of a tropical dry forest in Bolivia. *ISPRS J.*
712 *Photogramm. Remote Sens.* doi:10.1016/j.isprsjprs.2015.03.015
- 713 Dwyer, J., Roy, D., Sauer, B., Jenkerson, C., Zhang, H., Lymburner, L., 2018. Analysis Ready
714 Data: Enabling Analysis of the Landsat Archive 1–24.
715 doi:10.20944/PREPRINTS201808.0029.V1
- 716 Eckert, S., Hüsler, F., Liniger, H., Hodel, E., 2015. Trend analysis of MODIS NDVI time series for
717 detecting land degradation and regeneration in Mongolia. *J. Arid Environ.* 113, 16–28.
718 doi:10.1016/j.jaridenv.2014.09.001
- 719 Egorov, A. V., Roy, D.P., Zhang, H.K., Hansen, M.C., Kommareddy, A., 2018. Demonstration of

[This is a post-referring version]

[Accepted in *Remote Sensing of Environment*]

[DOI: 10.1016/j.rse.2019.111250]

[Link to the published paper: <https://doi.org/10.1016/j.rse.2019.111250>]

- 720 percent tree cover mapping using Landsat Analysis Ready Data (ARD) and sensitivity with
721 respect to Landsat ARD processing level. *Remote Sensing* 10. doi:10.3390/rs10020209
- 722 Erasmí, S., Schucknecht, A., Barbosa, M.P., Matschullat, J., 2014. Vegetation greenness in
723 northeastern Brazil and its relation to ENSO warm events. *Remote Sens.* 6, 3041–3058.
724 doi:10.3390/rs6043041
- 725 Evans, J., Geerken, R., 2004. Discrimination between climate and human-induced dryland
726 degradation. *J. Arid Environ.* 57, 535–554. doi:10.1016/S0140-1963(03)00121-6
- 727 Fensholt, R., Langanke, T., Rasmussen, K., Reenberg, A., Prince, S.D., Tucker, C., Scholes, R.J.,
728 Le, Q.B., Bondeau, A., Eastman, R., Epstein, H., Gaughan, A.E., Hellden, U., Mbow, C.,
729 Olsson, L., Paruelo, J., Schweitzer, C., Seaquist, J., Wessels, K., 2012. Greenness in semi-
730 arid areas across the globe 1981–2007 - an Earth Observing Satellite based analysis of
731 trends and drivers. *Remote Sensing of Environment.* 121, 144–158.
732 doi:10.1016/j.rse.2012.01.017
- 733 Flood, N., 2013. Seasonal composite Landsat TM/ETM+ Images using the medoid (a multi-
734 dimensional median). *Remote Sens.* 5, 6481–6500. doi:10.3390/rs5126481
- 735 Fontes Júnior, R.V. de P., Montenegro, A.A. de A., 2017. Temporal dependence of
736 potentiometric levels and groundwater salinity in alluvial aquifer upon rainfall and
737 evapotranspiration. *Rbrh* 22. doi:10.1590/2318-0331.0217170059
- 738 Funk, C., Peterson, P., Landsfeld, M., Pedreros, D., Verdin, J., Shukla, S., Husak, G., Rowland,
739 J., Harrison, L., Hoell, A., Michaelsen, J., 2015. The climate hazards infrared precipitation
740 with stations—a new environmental record for monitoring extremes. *Sci. Data* 2,
741 150066. doi:10.1038/sdata.2015.66
- 742 Gómez, C., White, J.C., Wulder, M.A., 2016. Optical remotely sensed time series data for land
743 cover classification: A review. *ISPRS Journal of Photogrammetry and Remote Sensing.*
744 doi:10.1016/j.isprsjprs.2016.03.008
- 745 Guan, K., Pan, M., Li, H., Wolf, A., Wu, J., Medvigy, D., Caylor, K.K., Sheffield, J., Wood, E.F.,
746 Malhi, Y., Liang, M., Kimball, J.S., Saleska, S.R., Berry, J., Joiner, J., Lyapustin, A.I., 2015.
747 Photosynthetic seasonality of global tropical forests constrained by hydroclimate. *Nat.*
748 *Geosci.* 8, 284–289. doi:10.1038/ngeo2382
- 749 He, C., Tian, J., Gao, B., Zhao, Y., 2015. Differentiating climate and human-induced drivers of
750 grassland degradation in the Liao River Basin, China. *Environ. Monit. Assess.* 187, 4199.
751 doi:10.1007/s10661-014-4199-2
- 752 Hein, L., De Ridder, N., Hiernaux, P., Leemans, R., De Wit, A., Schaepman, M., 2011.
753 Desertification in the Sahel: Towards better accounting for ecosystem dynamics in the
754 interpretation of remote sensing images. *Journal of Arid Environments.* 75, 1164–1172.
755 doi:10.1016/j.jaridenv.2011.05.002
- 756 Helsel, D.R., Hirsch, R.M., 2002. Trend Analysis. *Stat. Methods Water Resour. Tech. Water*
757 *Resour. Investig. B.* 4, chapter A3 323–355.
- 758 Higginbottom, T.P., Symeonakis, E., 2014. Assessing land degradation and desertification using

[This is a post-referring version]

[Accepted in *Remote Sensing of Environment*]

[DOI: 10.1016/j.rse.2019.111250]

[Link to the published paper: <https://doi.org/10.1016/j.rse.2019.111250>]

- 759 vegetation index data: Current frameworks and future directions. *Remote Sens.* 6, 9552–
760 9575. doi:10.3390/rs6109552
- 761 Holben, B.N., 1986. Characteristics of maximum-value composite images from temporal
762 AVHRR data. *Int. J. Remote Sens.* 7, 1417–1434. doi:10.1080/01431168608948945
- 763 Huete, A., Didan, K., Miura, T., Rodriguez, E.P., Gao, X., Ferreira, L.G., 2002. Overview
764 of the radiometric and biophysical performance of the MODIS vegetation indices.
765 *Remote Sens. Environ.* 83, 195–213. doi:10.1016/S0034-4257(02)00096-2
- 766 Huete, A.R., Liu, H.Q., Batchily, K., J., L. van W., 1997. A comparison of vegetation indices over
767 a global set of TM images for EOS-MODIS. *Remote Sensing of Environment*, 59(3), 440–
768 451. doi:10.1016/s0034-4257(96)00112-5.
- 769 Ibrahim, Y.Z., Balzter, H., Kaduk, J., Tucker, C.J., 2015. Land degradation assessment using
770 residual trend analysis of GIMMS NDVI3g, soil moisture and rainfall in Sub-Saharan West
771 Africa from 1982 to 2012. *Remote Sens.* 7, 5471–5494. doi:10.3390/rs70505471
- 772 IPCC. Intergovernmental Panel on Climate Change
773 http://www.ipcc.ch/ipccreports/sres/land_use/index.php?idp=157. Accessed in oct-
774 2018
- 775 Jacques, D.C., Kergoat, L., Hiernaux, P., Mougin, E., Defourny, P., 2014. Monitoring dry
776 vegetation masses in semi-arid areas with MODIS SWIR bands. *Remote Sens. Environ.*
777 153, 40–49. doi:10.1016/j.rse.2014.07.027
- 778 Jamali, S., Jönsson, P., Eklundh, L., Ardö, J., Seaquist, J., 2015. Detecting changes in vegetation
779 trends using time series segmentation. *Remote Sens. Environ.* 156, 182–195.
780 doi:10.1016/j.rse.2014.09.010
- 781 Jin, C., Xiao, X., Merbold, L., Arneeth, A., Veenendaal, E., Kutsch, W.L., 2013. Phenology and
782 gross primary production of two dominant savanna woodland ecosystems in Southern
783 Africa. *Remote Sens. Environ.* 135, 189–201. doi:10.1016/j.rse.2013.03.033
- 784 Ju, J., Masek, J.G., 2016. The vegetation greenness trend in Canada and US Alaska from 1984-
785 2012 Landsat data. *Remote Sensing of Environment*. doi:10.1016/j.rse.2016.01.001
- 786 Karlson, M., Ostwald, M., 2016. Remote sensing of vegetation in the Sudano-Sahelian zone: A
787 literature review from 1975 to 2014. *J. Arid Environ.* doi:10.1016/j.jaridenv.2015.08.022
- 788 Karnieli, A., Qin, Z., Wu, B., Panov, N., Yan, F., 2014. Spatio-temporal dynamics of land-use and
789 land-cover in the Mu Us Sandy Land, China, using the change vector analysis technique.
790 *Remote Sens.* 6, 9316–9339. doi:10.3390/rs6109316
- 791 Katsanos, D., Retalis, A., Michaelides, S., 2016. Validation of a high-resolution precipitation
792 database (CHIRPS) over Cyprus for a 30-year period. *Atmos. Res.* 169, 459–464.
793 doi:10.1016/j.atmosres.2015.05.015
- 794 Lambin, E.F., Geist, H.J., Lepers, E., 2003. Dynamics of land use and land cover change in
795 tropical regions. *Annu. Rev. Environ. Resour.* 28, 205–241.
796 doi:10.1146/annurev.energy.28.050302.105459

[This is a post-referring version]

[Accepted in *Remote Sensing of Environment*]

[DOI: 10.1016/j.rse.2019.111250]

[Link to the published paper: <https://doi.org/10.1016/j.rse.2019.111250>]

- 797 Lamchin, M., Lee, J.Y., Lee, W.K., Lee, E.J., Kim, M., Lim, C.H., Choi, H.A., Kim, S.R., 2016.
798 Assessment of land cover change and desertification using remote sensing technology
799 in a local region of Mongolia. *Adv. Sp. Res.* 57, 64–77.
800 doi:10.1016/j.asr.2015.10.006
- 801 Le Toan, T., Quegan, S., Davidson, M.W.J., Balzter, H., Paillou, P., Papathanassiou, K., Plummer,
802 S., Rocca, F., Saatchi, S., Shugart, H., Ulander, L., 2011. The BIOMASS mission: Mapping
803 global forest biomass to better understand the terrestrial carbon cycle. *Remote Sens.*
804 *Environ.* 115, 2850–2860. doi:10.1016/j.rse.2011.03.020
- 805 Leal, I.R., Da Silva, J.M.C., Tabarelli, M., Lacher, T.E., 2005. Changing the Course of Biodiversity
806 Conservation in the Caatinga of Northeastern Brazil\Cambiando el Curso de la
807 Conservación de Biodiversidad en la Caatinga del Noreste de Brasil. *Conserv. Biol.* 19,
808 701–706. doi:10.1111/j.1523-1739.2005.00703.x
- 809 Leroux, L., Bégué, A., Lo Seen, D., Jolivot, A., Kayitakire, F., 2017. Driving forces of recent
810 vegetation changes in the Sahel: Lessons learned from regional and local level analyses.
811 *Remote Sens. Environ.* 191, 38–54. doi:10.1016/j.rse.2017.01.014
- 812 Li, X.B., Li, R.H., Li, G.Q., Wang, H., Li, Z.F., Li, X., Hou, X.Y., 2016. Human-induced vegetation
813 degradation and response of soil nitrogen storage in typical steppes in Inner Mongolia,
814 China. *Journal of Arid Environments.* doi:10.1016/j.jaridenv.2015.07.013
- 815 Lima, A.L.A., Rodal, M.J.N., 2010. Phenology and wood density of plants growing in the semi-
816 arid region of northeastern Brazil, *Journal of Arid Environments.*
817 doi:10.1016/j.jaridenv.2010.05.009
- 818 Lima, G.D.S., Lima, J.R. de F., Silva, N. da, Oliveira, R.S. de, Lucena, R.F.P., 2016. Inventory in
819 situ of plant resources used as fuel in the Semiarid Region of Northeast Brazil. *Brazilian*
820 *J. Biol. Sci.* 3, 45. doi:10.21472/bjbs.030505
- 821 Linares-Palomino, R., Oliveira-Filho, A.T., Pennington, R.T., 2011. Seasonally Dry Tropical
822 Forests 3–21. doi:10.5822/978-1-61091-021-7
- 823 Liu, F., Chen, Y., Lu, H., Shao, H., 2017. Albedo indicating land degradation around the Badain
824 Jaran Desert for better land resources utilization. *Sci. Total Environ.* 578, 67–73.
825 doi:10.1016/j.scitotenv.2016.06.171
- 826 Liu, J., Shao, Q., Yan, X., Fan, J., Zhan, J., Deng, X., Huang, L, 2016. The climatic impacts of land
827 use and land cover change compared among countries. *Journal of Geographical*
828 *Sciences*, 26(7), 889–903. doi: 10.1007/s11442-016-1305-0
- 829 Loveland, T.R., Dwyer, J.L., 2012. Landsat: Building a strong future. *Remote Sensing of*
830 *Environment.* 122, 22–29. doi:10.1016/j.rse.2011.09.022
- 831 Marengo, J.A., Torres, R.R., Alves, L.M., 2017. Drought in Northeast Brazil—past, present, and
832 future. *Theor. Appl. Climatol.* 129, 1189–1200. doi:10.1007/s00704-016-1840-8
- 833 Mariano, D.A., Santos, C.A.C. do., Wardlow, B.D., Anderson, M.C., Schiltmeyer, A. V., Tadesse,
834 T., Svoboda, M.D., 2018. Use of remote sensing indicators to assess effects of drought
835 and human-induced land degradation on ecosystem health in Northeastern Brazil.

[This is a post-referring version]

[Accepted in *Remote Sensing of Environment*]

[DOI: 10.1016/j.rse.2019.111250]

[Link to the published paper: <https://doi.org/10.1016/j.rse.2019.111250>]

- 836 Remote Sens. Environ. 213, 129–143. doi:10.1016/j.rse.2018.04.048
- 837 Mas, 1999. International Journal of Monitoring land-cover changes : A comparison of change
838 detection techniques. *Int. J. Remote Sens.* 20, 139–152. doi:10.1080/014311699213659
- 839 Masek, J.G., Vermote, E.F., Saleous, N.E., Wolfe, R., Hall, F.G., Huemmrich, K.F., Gao, F., Kutler,
840 J., Lim, T., 2006. A Landsat Surface Reflectance Dataset for North America, 1990–2000.
841 *IEEE Geoscience and Remote Sensing Letters*, 3(1), 68–72. doi:10.1109/lgrs.2005.857030
- 842 Matthias, A.D.D., Fimbres, A., Sano, E.E.E., Post, D.F.F., Accioly, L., Batchily, A.K.K., Ferreira,
843 L.G.G., 2000. Surface roughness effects on soil albedo. *Soil Sci. Soc. Am. J.* 64, 1035–
844 1041. doi:10.2136/sssaj2000.6431035x
- 845 Mayes, M.T., Mustard, J.F., Melillo, J.M., 2015. Forest cover change in Miombo Woodlands:
846 Modeling land cover of African dry tropical forests with linear spectral mixture analysis.
847 *Remote Sens. Environ.* 165, 203–215. doi:10.1016/j.rse.2015.05.006
- 848 Medeiros, I.C., da Costa Silva, J.F.C.B., Silva, R.M., Santos, C.A.G., 2018. Run-off–erosion
849 modelling and water balance in the Epitácio Pessoa Dam river basin, Paraíba State in
850 Brazil. *Int. J. Environ. Sci. Technol.* doi:10.1007/s13762-018-1940-3
- 851 MMA, Brazilian Ministry of the Environment, 2018. <http://geocatalogo.mma.gov.br/>
- 852 Moro, M.F., Lughadha, E.N., Araújo, F.S. De, Martins, F.R., 2016. A Phytogeographical
853 Metaanalysis of the Semiarid Caatinga Domain in Brazil. *Bot. Rev.* doi:10.1007/s12229-
854 016-9164-z
- 855 Moro, M.F., Nic Lughadha, E., de Araújo, F.S, 2016. *Bot. Rev.* 82: 91. doi: 10.1007/s12229-016-
856 9164-z
- 857 Munyati, C., Mboweni, G., 2013. Variation in NDVI values with change in spatial resolution for
858 semi-arid savanna vegetation: A case study in northwestern South Africa. *Int. J. Remote*
859 *Sens.* 34, 2253–2267. doi:10.1080/01431161.2012.743692
- 860 Nagler, P.L., Daughtry, C.S.T., Goward, S.N., 2000. Plant litter and soil reflectance. *Remote*
861 *Sens. Environ.* 71, 207–215. doi:10.1016/S0034-4257(99)00082-6
- 862 National Institute of Meteorology of Brazil, 2018. Available:
863 <http://www.inmet.gov.br/portal/index.php?r=bdmep/bdmep>
- 864 Nouvelot, J. F. 1974. Planificação da implantação de bacias representativas. Recife, SUDENE-
865 DRN.
- 866 Padilha, A. L., Vitorello, Í., Pádua, M. B., & Fuck, R. A, 2016. Deep magnetotelluric signatures
867 of the early Neoproterozoic Cariris Velhos tectonic event within the Transversal sub-
868 province of the Borborema Province, NE Brazil. *Precambrian Research*, 275, 70-83.
- 869 Paredes-Trejo, F.J., Barbosa, H.A., Lakshmi Kumar, T. V., 2017. Validating CHIRPS-based
870 satellite precipitation estimates in Northeast Brazil. *J. Arid Environ.* 139, 26–40.
871 doi:10.1016/j.jaridenv.2016.12.009
- 872 Pereira, I.M., Andrade, L.A., Sampaio, E.V.S.B., Barbosa, M.R. V., 2003. Use-history Effects on

[This is a post-referring version]

[Accepted in *Remote Sensing of Environment*]

[DOI: 10.1016/j.rse.2019.111250]

[Link to the published paper: <https://doi.org/10.1016/j.rse.2019.111250>]

- 873 Structure and Flora of Caatinga. *Biotropica* 35, 154–165. doi:10.1111/j.1744-
874 7429.2003.tb00275.x
- 875 Perez-Marin, Aldrin & Cavalcante, A.M.B. & Medeiros, Silvana & Tinôco, Leonardo & Salcedo,
876 I.H. 2012. Núcleos de desertificação no semiárido brasileiro: Ocorrência natural ou
877 antrópica?. *Parcerias Estratégicas*. 17. 87-106.
- 878 Perugini, L., Caporaso, L., Marconi, S., Cescatti, A., Quesada, B., de Noblet-Ducoudré, N., ...
879 Arneeth, A. 2017. Biophysical effects on temperature and precipitation due to land cover
880 change. *Environmental Research Letters*, 12(5), 053002. doi: 10.1088/1748-
881 9326/aa6b3f
- 882 Pinheiro, E.A.R., Costa, C.A.G., De Araújo, J.C., 2013. Effective root depth of the Caatinga
883 biome. *J. Arid Environ.* 89, 1–4. doi:10.1016/j.jaridenv.2012.10.003
- 884 R Core Team, 2017. R: A language and environment for statistical computing. R Foundation
885 for Statistical Computing, Vienna, Austria. URL <https://www.R-project.org/>.
- 886 Rodal, M., Barbosa, M., Thomas, W., 2008. Do the seasonal forests in northeastern Brazil
887 represent a single floristic unit? *Brazilian J. Biol.* 68, 467–475. doi:10.1590/S1519-
888 69842008000300003
- 889 Rodríguez-Caballero, E., Knerr, T., Weber, B., 2015. Importance of biocrusts in dryland
890 monitoring using spectral indices. *Remote Sens. Environ.* 170, 32–39.
891 doi:10.1016/j.rse.2015.08.034
- 892 Saco, P.M., Moreno-de las Heras, M., Keesstra, S., Baartman, J., Yetemen, O., Rodríguez, J.F.,
893 2018. Vegetation and soil degradation in drylands: Non linear feedbacks and early
894 warning signals. *Curr. Opin. Environ. Sci. Heal.* 5, 67–72.
895 doi:10.1016/j.coesh.2018.06.001
- 896 Salcedo, I.H., Tiessen, H., Sampaio, E.V.S.B., 1997. Nutrient availability in, soil samples from
897 shifting cultivation sites in the semi-arid Caatinga of NE Brazil. *Agric. Ecosyst. Environ.*
898 65, 177–186. doi:10.1016/S0167-8809(97)00073-X
- 899 Samain, O., Kergoat, L., Hiernaux, P., Guichard, F., Mougín, E., Timouk, F., Lavenu, F., 2008.
900 Analysis of the in situ and MODIS albedo variability at multiple timescales in the sahel. *J.*
901 *Geophys. Res. Atmos.* 113, 1–16. doi:10.1029/2007JD009174
- 902 Sanderson M., Pope E., Santini M., Mercogliano P., Montesarchio, M., 2012 Influences of EU
903 forests on weather patterns: Final Report. Report for the European commission (DG-
904 Environment).
905 http://ec.europa.eu/environment/forests/pdf/EU_Forests_Final_Report.pdf
- 906 Santos, a M., Tabarelli, M., 2002. Distance from roads and cities as a predictor of habitat loss
907 and fragmentation in the caatinga vegetation of Brazil. *Braz. J. Biol.* 62, 897–905.
908 doi:10.1590/S1519-69842002000500020
- 909 Santos, R.M., Oliveira-Filho, A.T., Eisenlohr, P. V., Queiroz, L.P., Cardoso, D.B.O.S., Rodal,
910 M.J.N., 2012. Identity and relationships of the Arboreal Caatinga among other floristic
911 units of seasonally dry tropical forests (SDTFs) of north-eastern and Central Brazil,

[This is a post-referring version]

[Accepted in *Remote Sensing of Environment*]

[DOI: 10.1016/j.rse.2019.111250]

[Link to the published paper: <https://doi.org/10.1016/j.rse.2019.111250>]

- 912 Ecology and Evolution. doi:10.1002/ece3.91
- 913 Savitzky, A., Golay, M.J.E., 1964. Smoothing and Differentiation of Data by Simplified Least
914 Squares Procedures. *Anal. Chem.* 36, 1627–1639. doi:10.1021/ac60214a047
- 915 Schertz, T., Alexander, R., Ohe, D., 1991. The computer program Estimate Trend (ESTREND), a
916 system for the Detection of Trends in Water-quality data 1–63.
- 917 Schucknecht, A., Erasmi, S., Niemeyer, I., Matschullat, J., 2013. Assessing vegetation variability
918 and trends in north-eastern Brazil using AVHRR and MODIS NDVI time series. *European*
919 *Journal of Remote Sensing.* 46, 40–59. doi:10.5721/EuJRS20134603
- 920 Schwinning, S., Sala, O.E., Loik, M.E., 2004 *Oecologia* 141: 191. doi: 10.1007/s00442-004-
921 1683-3
- 922 Shuai, Y., Masek, J.G., Gao, F., Schaaf, C.B., 2011. An algorithm for the retrieval of 30-m snow-
923 free albedo from Landsat surface reflectance and MODIS BRDF. *Remote Sens. Environ.*
924 115, 2204–2216. doi:10.1016/j.rse.2011.04.019
- 925 Shuai, Y., Masek, J.G., Gao, F., Schaaf, C.B., He, T., 2014. An approach for the long-term 30-m
926 land surface snow-free albedo retrieval from historic Landsat surface reflectance and
927 MODIS-based a priori anisotropy knowledge. *Remote Sens. Environ.* 152, 467–479.
928 doi:10.1016/j.rse.2014.07.009
- 929 Silva JMC, Barbosa LCF, Leal, IR. Tabarelli M, 2017 The Caatinga: Understanding the
930 Challenges. Silva JMC, Leal IR, Tabarelli M, editors. *Caatinga: the largest tropical dry*
931 *forest region in South America.* Cham: Springer; doi: 10.1007/978-3-319-68339-3_1
- 932 Silva, G.C., Sampaio, E.V.S.B., 2008. Biomassas de partes aéreas em plantas da Caatinga. *Soc.*
933 *Investig. Florestais* 32, 567–575. doi:10.1016/j.jaridenv.2015.02.003
- 934 Sobrinho, M. S., Tabarelli, M. , Machado, I. C., Sfair, J. C., Bruna, E. M. and Lopes, A. V. 2016.
935 Land use, fallow period and the recovery of a Caatinga forest. *Biotropica*, 48:586-597.
936 doi:10.1111/btp.12334
- 937 Song, X.P., Huang, C., Sexton, J.O., Channan, S., Townshend, J.R., 2014. Annual detection of
938 forest cover loss using time series satellite measurements of percent tree cover. *Remote*
939 *Sensing.* 6, 8878–8903. doi:10.3390/rs6098878
- 940 Steyaert, L. T., & Knox, R. G, 2008. Reconstructed historical land cover and biophysical
941 parameters for studies of land-atmosphere interactions within the eastern United
942 States. *Journal of Geophysical Research*, 113(D2), D02101. doi: 10.1029/2006JD008277
- 943 Stroppiana, D., Bordogna, G., Carrara, P., Boschetti, M., Boschetti, L., Brivio, P.A., 2012. A
944 method for extracting burned areas from Landsat TM/ETM+ images by soft aggregation
945 of multiple Spectral Indices and a region growing algorithm. *ISPRS J. Photogramm.*
946 *Remote Sens.* 69, 88–102. doi:10.1016/j.isprsjprs.2012.03.001
- 947 Torrence, C., Compo, G.P., 1998. A practical guide to wavelet analysis. *Bull. Am. Meteor. Soc.*
948 79, 61–78. doi:10.1175/1520-0477(1998)079<0061:APGTWA>2.0.CO;2
- 949 Tucker, C.J., 1979. Red and photographic infrared linear combinations for monitoring

[This is a post-referring version]

[Accepted in *Remote Sensing of Environment*]

[DOI: 10.1016/j.rse.2019.111250]

[Link to the published paper: <https://doi.org/10.1016/j.rse.2019.111250>]

- 950 vegetation. *Remote Sens. Environ.* 8, 127–150. doi:10.1016/0034-4257(79)90013-0
- 951 U.S. Geological Survey, 2018a. Product Guide: LANDSAT 4-7 SURFACE REFLECTANCE (LEDAPS)
952 PRODUCT. Department of the Interior Version 8.3,
953 https://landsat.usgs.gov/sites/default/files/documents/ledaps_product_guide.pdf
- 954 U.S. Geological Survey, 2018b. Product Guide: Landsat 8 Surface Reflectance code (LaSRC)
955 product. Department of the Interior Version 4.3,
956 https://landsat.usgs.gov/sites/default/files/documents/lasrc_product_guide.pdf
- 957 Velloso, A. L., Sampaio, E. V. S. B., & Pareyn, F. G. C, 2001. Ecorregiões: propostas para o bioma
958 caatinga; resultados do seminário de planejamento ecorregional da caatinga. Seminário
959 de Planejamento Ecorregional da Caatinga. TNC/APNE Recife, Aldeia-Pernambuco, 76.
- 960 Verbesselt, J., Hyndman, R., Newnham, G., Culvenor, D., 2010. Detecting trend and seasonal
961 changes in satellite image time series. *Remote Sens. Environ.*
962 doi:10.1016/j.rse.2009.08.014
- 963 Verbesselt, J., Umlauf, N., Hirota, M., Holmgren, M., Van Nes, E.H., Herold, M., Zeileis, A.,
964 Scheffer, M., 2016. Remotely sensed resilience of tropical forests. *Nat. Clim. Chang.*
965 doi:10.1038/nclimate3108
- 966 Verbesselt, J., Zeileis, A., Herold, M., 2012. Near real-time disturbance detection using
967 satellite image time series. *Remote Sens. Environ.* doi:10.1016/j.rse.2012.02.022
- 968 Vermote, E., Justice, C., Claverie, M., Franch, B., 2016. Remote Sensing of Environment
969 Preliminary analysis of the performance of the Landsat 8 / OLI land surface reflectance
970 product. *Remote Sens. Environ.* doi:10.1016/j.rse.2016.04.008
- 971 Vicente-Serrano S.M., Beguería, S. López-Moreno, J.I., 2010. A Multi-scalar drought index
972 sensitive to global warming: The Standardized Precipitation Evapotranspiration Index -
973 SPEI. *Journal of Climate* 23, 1696-1718. <https://doi.org/10.1175/2009JCLI2909.1>
- 974 Walker, J., de Beurs, K., Wynne, R.H., 2015. Phenological response of an Arizona dryland forest
975 to short-term climatic extremes. *Remote Sens.* 7, 10832–10855.
976 doi:10.3390/rs70810832
- 977 Wang, Z., Erb, A.M., Schaaf, C.B., Sun, Q., Liu, Y., Yang, Y., Shuai, Y., Casey, K.A., Román, M.O.,
978 2016. Remote Sensing of Environment Early spring post-fire snow albedo dynamics in
979 high latitude boreal forests using Landsat-8 OLI data. *Remote Sens. Environ.* 185, 71–83.
980 doi:<http://dx.doi.org/10.1016/j.rse.2016.02.059>
- 981 Wang, Z., Schaaf, C.B., Sun, Q., Kim, J., Erb, A.M., Gao, F., Román, M.O., Yang, Y., Petroy, S.,
982 Taylor, J.R., Masek, J.G., Morisette, J.T., Zhang, X., Papuga, S.A., 2017. Monitoring land
983 surface albedo and vegetation dynamics using high spatial and temporal resolution
984 synthetic time series from Landsat and the MODIS BRDF/NBAR/albedo product.
985 *International Journal of Applied Earth Observation and Geoinformation.*
986 doi:10.1016/j.jag.2017.03.008
- 987 Wessels, K.J., Prince, S.D., Malherbe, J., Small, J., Frost, P.E., VanZyl, D., 2007. Can human-
988 induced land degradation be distinguished from the effects of rainfall variability? A case

[This is a post-referring version]

[Accepted in *Remote Sensing of Environment*]

[DOI: 10.1016/j.rse.2019.111250]

[Link to the published paper: <https://doi.org/10.1016/j.rse.2019.111250>]

- 989 study in South Africa. *J. Arid Environ.* 68, 271–297. doi:10.1016/j.jaridenv.2006.05.015
- 990 Wessels, K.J., van den Bergh, F., Scholes, R.J., 2012. Limits to detectability of land degradation
991 by trend analysis of vegetation index data. *Remote Sens. Environ.* 125, 10–22.
992 doi:10.1016/j.rse.2012.06.022
- 993 Wulder, M.A., White, J.C., Loveland, T.R., Woodcock, C.E., Belward, A.S., Cohen, W.B.,
994 Fosnight, E.A., Shaw, J., Masek, J.G., Roy, D.P., 2016. The global Landsat archive: Status,
995 consolidation, and direction. *Remote Sensing of Environment.* 185, 271–283.
996 doi:10.1016/j.rse.2015.11.032
- 997 Xu, D., Guo, X., Li, Z., Yang, X., Yin, H., 2014. Remote Sensing of Environment Measuring the
998 dead component of mixed grassland with Landsat imagery. *Remote Sens. Environ.* 142,
999 33–43. doi:10.1016/j.rse.2013.11.017
- 1000 Yang, Y., Wang, Z., Li, J., Gang, C., Zhang, Y., Zhang, Y., Odeh, I., Qi, J., 2016. Comparative
1001 assessment of grassland degradation dynamics in response to climate variation and
1002 human activities in China, Mongolia, Pakistan and Uzbekistan from 2000 to 2013. *Journal
1003 of Arid Environments.* 135, 164–172. doi:10.1016/j.jaridenv.2016.09.004
- 1004 Yu, Y., Notaro, M., Wang, F., Mao, J., Shi, X., Wei, Y., 2017. Observed positive vegetation-
1005 rainfall feedbacks in the Sahel dominated by a moisture recycling mechanism. *Nat.
1006 Commun.* 8, 1–9. doi:10.1038/s41467-017-02021-1
- 1007 Zhang, J., Niu, J.M., Bao, T., Buyantuyev, A., Zhang, Q., Dong, J.J., Zhang, X.F., 2014. Human
1008 induced dryland degradation in Ordos Plateau, China, revealed by multilevel statistical
1009 modeling of normalized difference vegetation index and rainfall time-series. *J. Arid Land*
1010 6, 219–229. doi:10.1007/s40333-013-0203-x
- 1011 Zhao, Y., Wang, X., Novillo, C.J., Arrogante-Funes, P., Vázquez-Jiménez, R., Maestre, F.T., 2018.
1012 Albedo estimated from remote sensing correlates with ecosystem multifunctionality in
1013 global drylands. *J. Arid Environ.* 157, 116–123. doi:10.1016/j.jaridenv.2018.05.010
- 1014
- 1015